Compressed Sensing based underwater acoustic channel estimation using two dimensional frequency characterization

Naushad Ansari

IIIT-D-MTech-ECE
December 14, 2016

Indraprastha Institute of Information Technology
New Delhi

Thesis Advisors

Dr. Anubha Gupta (IIIT-Delhi)

Dr. Ananya Sen Gupta (Univ. of Iowa, USA)

Examiners

Dr. Monika Aggarwal (IIT-Delhi)

Dr. Sanjit Krishnan Kaul (IIIT-Delhi)

Submitted in partial fulfillment of the requirements
for the Degree of M.Tech. in Electronics & Communication,
with specialization in Communication & Signal Processing

Certificate

This is to certify that the thesis titled **" Compressed Sensing based underwater acoustic channel estimation using two dimensional frequency characterization"** submitted by **Naushad Ansari** for the partial fulfillment of the requirements for the degree of *Master of Technology* in *Electronics & Communication Engineering* is a record of the bonafide work carried out by him under my guidance and supervision at Indraprastha Institute of Information Technology, Delhi. This work has not been submitted anywhere else for the reward of any other degree.

Dr. Anubha Gupta
Indraprastha Institute of Information Technology, New Delhi, India

Dr. Ananya Sen Gupta
University of Iowa, Iowa, U.S.A.

Acknowledgments

I want to extend my heartfelt gratitude to my guides Dr. Anubha Gupta and Dr. Ananya Sen Gupta for their constant support throughout my thesis. They consistently gave me time for detailed technical discussions even after their busy schedule. Their guidance and motivation made me successfully complete my thesis.

I would like to thank Council of Scientific and Industrial Research (CSIR) for their financial support. I would like to thank all the members of IIIT-Delhi for providing such a great working atmosphere.

Also, I heartily thank my mother, sister and brothers for their consistent support in all events of my life. I could not reach at this stage without their support.

I thank my lab members (Hemant Kr. Aggarwal, Hemanta Kr. Mondal, Wazir Singh, Shiju S.) for encouraging me to work harder. Specifically, I am thankful to Hemant Kr. Aggarwal for his continuous technical and non-technical suggestions and helping at all the odd paths during my work. This would not have been possible without his support.

Contents

List of Figures

Abstract

Underwater acoustic (UWA) channel estimation in shallow water depths is a challenging problem due to rapidly fluctuating transients in the acoustic channel impulse response. Transmitted signal undergoes nonstationary reflections at the moving sea surface and rough sea bottom before being received via multiple paths at the receiver. These non-stationary reflections along with unpredictable surges of energy due to surface focusing events render the channel delay spread challenging to localize. In this work, we present compressed sensing (CS) based underwater acoustic channel estimation techniques at the intersection of time, frequency and sparsity. Specifically, following are the key contributions of this work.

First, a 2D frequency domain representation of the channel is obtained via a carefully chosen transmitted signal design. This modeling transforms the problem of channel estimation to channel recovery in 2D Fourier domain. Interestingly, this framework is similar to K-space based image reconstruction used in Magnetic Resonance Imaging (MRI) where CS is used extensively for signal recovery. It is observed that the channel is sparser in the 2D Fourier domain in comparison to the channel in time domain. Thus, the proposed frequency domain representation allows CS framework to be inherited naturally. Here, it is pertinent to add that this framework has been proposed for the first time in UWA.

Second, we introduce non-uniform compressing sampling for shallow water acoustic communications. Specifically, techniques presented in this work perform random CS at different sampling rates across different frequency bands in the 2D frequency domain. We propose non-uniform CS with prior information and non-uniform modified-CS with the prior information method for channel estimation wherein application domain knowledge is utilized with reference to frequency domain characteristics of the shallow water channel. Thus, this work illustrates the use of CS methods but by appropriately rooting them in this application domain.

We present numerical validation of proposed techniques based on channel estimates from field experiments as well as a public domain channel simulator that has recently been tested against data from different field trials.

Chapter 1

Introduction

Undersea communications and related signal processing techniques have been richly investigated over the last few decades [2, 3, 7, 12–17]. Despite phenomenal advancements in underwater acoustic propagation models and related channel representations [17, 18], a fundamental challenge to underwater acoustic communications is robust real-time estimation of underwater channel, which manifests rapidly fluctuating multipath channel effects due to transient oceanic surface wave activity, as well as slowly varying multipath components from relatively steady-state reflections between the moving sea surface and sea bottom. These diverse multipath effects due to oceanic activity render traditional adaptive channel estimation techniques challenging to implement using traditional sparse sensing or least squared error minimization techniques. This is primarily due to the three-way uncertainty principle of time, frequency, and sparsity that interacts with two important aspects of the channel delay spread:

(i) high-energy transients in the channel activity: These occur due to surface wave focusing events and follow a heavy-tailed distribution that is best observed in short time intervals and recovered using sparse sensing techniques [5–7]; and

(ii) slowly varying channel components: These occur due to relatively steady specular multipath reflections and diffused reflections from rough sea bottoms and follow a non-sparse distribution that needs to be observed over longer periods of time for precise estimation. These are best recovered by traditional least-square techniques [8, 9].

The three-way uncertainty is articulated in [10]. The three-way uncertainty involving time, frequency, and sparsity provides localization challenges for direct application of sparse sensing methods with appropriate observation windows. As such, precise localization of the shallow water channel in time, frequency and sparsity is not possible without precise real-time knowledge of ocean ground truths that is impractical to determine in real-life experiments. Therefore, there is a need for suitable formulation that is able to localize the dominant components of the shallow water channel robustly in real time for better channel estimation. This work is aimed to address this fundamental localization and channel estimation challenge. Specifically,

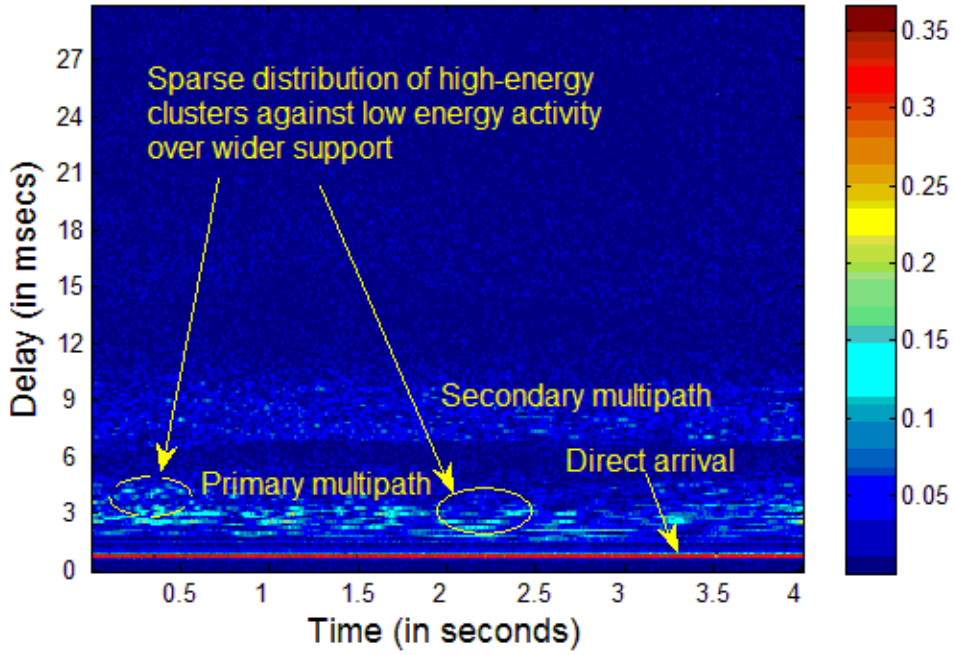

Figure 1.1: Shallow water acoustic channel (estimated from field data of SPACE08 experiment [1]), plotted as a two-dimensional image (Delay vs. Time) showing significant time-variability in primary and secondary multipath regions. High-energy clusters of delay spread components in the primary multipath region are also pointed out. Note: Colorbar is linear.

the inherent physical properties of multipath within the shallow water channel are harnessed with adaptive sparse sensing approaches and partial sampling methods.

1.1 Different components of channel delay spread

Reflections from the moving ocean surface as well as the sea bottom, which functions as a diffuse reflector, lead to multipath arrivals from the transmitter to the receiver. This results in a non-stationary time-varying channel impulse response, popularly referred to as the delay spread [2, 3, 7, 12–15, 17], which typically stretches over 100-200 delay taps (e.g. refer to results from experimental field data in [2]).

Fig. 1.1 * shows a typical time-varying delay spread (∼30 milliseconds long) of an underwater acoustic channel (estimated every 7.7 msecs duration using non-convex mixed norm solver (NCMNS) algorithm [2] from field data of SPACE08 experiment, section II of [1]) at 15 meters depth and 200 meters range. Delay refers to delay taps constituting the channel impulse response at a given point in time on the x-axis. The direct arrival path, the primary multipath

*Units in figure are in volts, or equivalently in micropascals (With appropriate conversion factor) depending on whether we consider channel as end-to-end from transmitter-transducer-channel-transducer-receiver or just the acoustic channel itself. Usually the conversion factor is suppressed in underwater literature and hence, delay spread coefficients, i.e., channel taps, are shown as unitless, with default being volts.

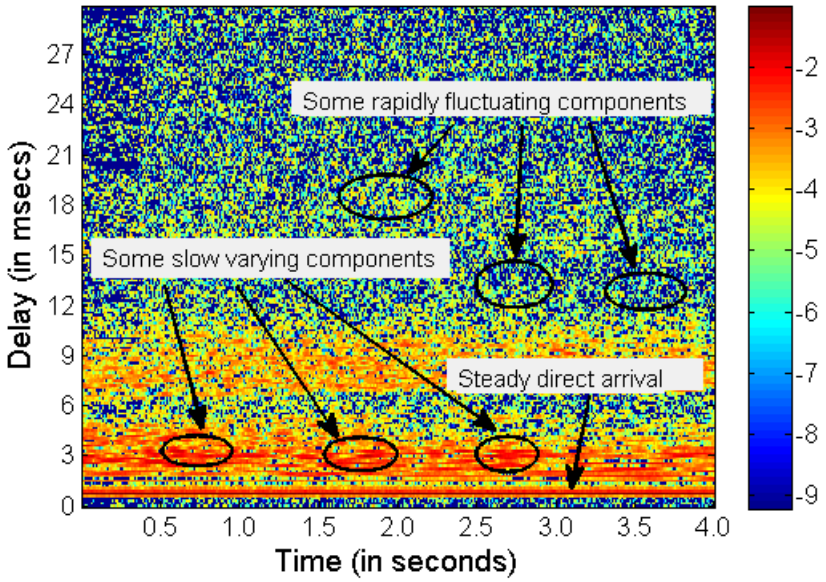

Figure 1b: Shallow water acoustic channel (estimated from field data of SPACE08 experiment [1]), plotted as a two-dimensional image (Delay vs. Time) corresponding to Fig. 1 above with log scale colorbar.

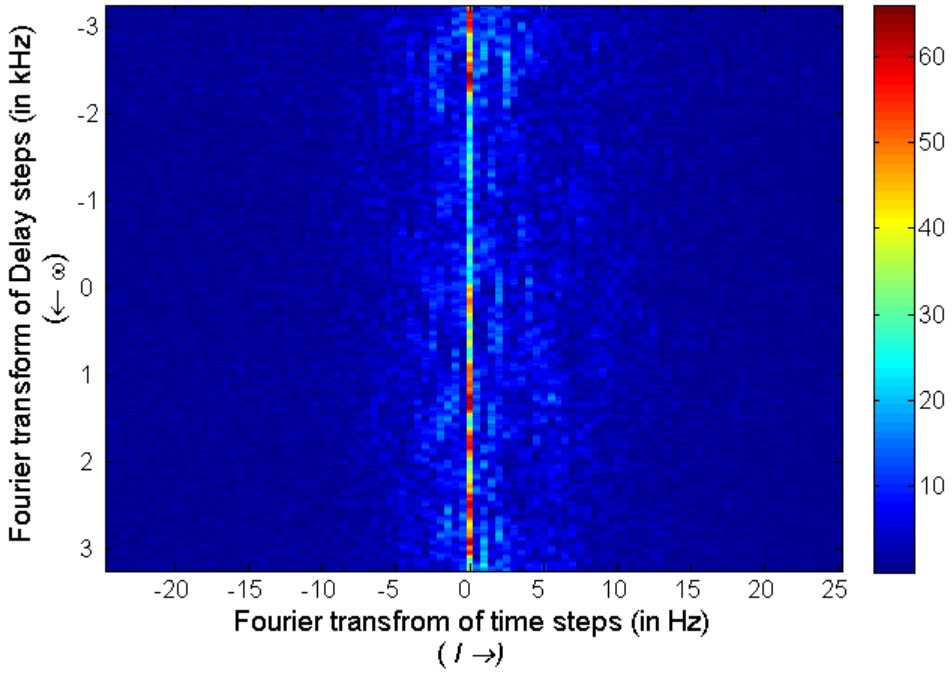

Figure 1.2: 2-D Fourier Transform of channel in baseband (estimated from field data of SPACE08 experiment [1]) shown in Fig. 1.1; Note: Colorbar is linear.

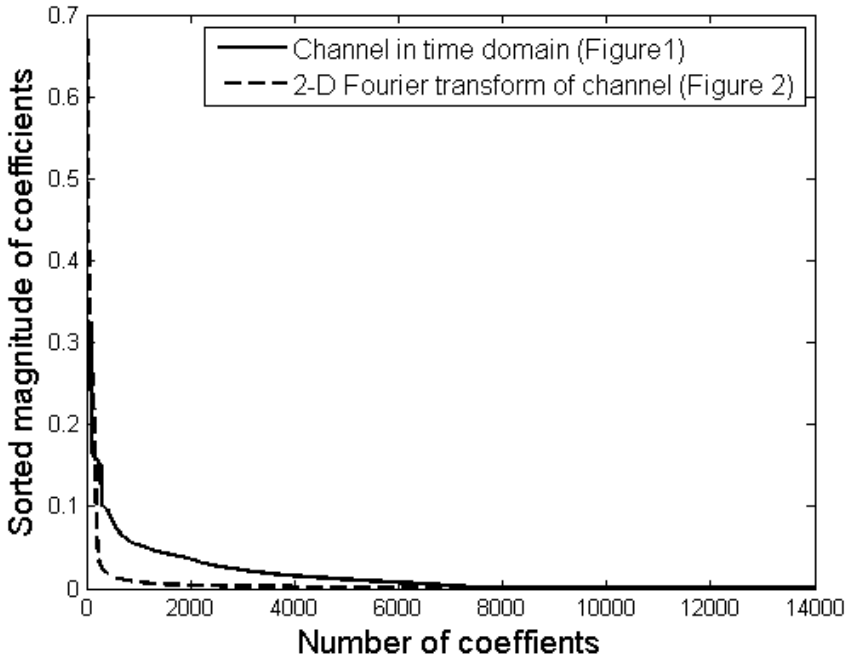

Figure 1.3: Sorted magnitude coefficients of 2-D time domain channel shown in Fig. 1.1 and 2-D Fourier transform of channel shown in Fig. 1.2.

region, and the secondary multipath region are marked in Fig. 1.1.

This is to note that the channel delay spread comprises of three distinct arrival regions:

1. The direct arrival representing the line-of-sight arrival of the acoustic waves from the transmitter to the receiving hydrophone. The direct arrival path manifests as the steady bright line at the bottom of Fig. 1.1, and is relatively constant over time, unless there is relative motion between the transmitter and receiver;

2. Primary multipath reflections that are, typically, the combined effect of one or a few surface wave reflections [2,7,10]. These delay taps, henceforth referred to as the primary delay taps, are highly transient in nature. They occupy a significant fraction of the channel energy and support, and occasionally exhibit high-energy peaks [19] and transient oceanographic events. Primary multipath is highlighted in Fig. 1.1; and

3. Secondary multipath reflections resulting from several reflections between the moving ocean surface and sea bottom. Due to attenuation at each reflection, these multipath arrivals do not have large energy within the delay spread, but collectively constitute a significant portion of the channel support. The secondary multipath arrivals are more relevant over medium range (200-1000 m) and shallow water depths as greater water depths and longer ranges attenuate their energy to ambient noise levels.

1.2 Uncertainly principles dictating underlying channel tap distribution

Non-stationary shifts in the channel delay spread due to oceanographic fluctuations limit the ability of adaptive signal processing techniques, with and without sparsity constraints, to track the shallow water channel in real time. In particular, uncertainty principle dictating localization of the non-stationary channel delay spread in time and frequency need to further consider the shifting sparseness of channel support [10]. The three-way uncertainty involving time, frequency and sparsity across the transient delay taps render direct application of sparse sensing methods challenging in the shallow water domain. This is particularly true under moderate to rough sea conditions. Data-driven evidence of the shifting sparsity has been provided in [20].

1.3 Summary of related work and scope

The scope of this work is geared towards real-time channel estimation over medium ranges and shallow water depths. The focus of this work is on the medium range because the joint effect of the primary and secondary multipath arrivals are most pronounced in this paradigm and hence, this is the more daunting scenario to solve. To provide field-driven evidence to the proposed methods, channel ground truths derived from experimental field data collected at 200 meters range and 15 meters depth are chosen as a representative scenario for this paradigm.

Localization of time-varying channel delay spread is challenging due to rapidly fluctuating multipath arrivals discussed in section 1.1 and uncertainty principles governing localization as discussed in section 1.2 Current state-of-the-art in shallow water channel estimation addresses these challenges in four complementary thrusts:

1. Non-uniform methods that attempt to discover and predict the shallow water channel using ray theory models [7, 21];
2. Adaptive signal processing methods based on least-squared techniques [7, 15, 22];
3. Sparse recovery methods in optimization framework that exploit the sparse support of high-energy transients [6, 23, 24]; and
4. Channel estimation using MIMO framework [6, 23, 25].

Sparse recovery methods [26–28] are well-known to provide improvements over traditional adaptive least squares techniques [9], when the signal to be recovered has sparse support. In such scenarios, regularization terms are added as constraints in the optimization framework to enable signal recovery [29]. Sparse recovery methods are closely tied but separate from Compressive Sampling/Compressed Sensing (CS) [5, 30–32] techniques that solve the problem of signal recovery from underdetermined system of linear equations under sparsity constraint. Recently, OMP (Orthogonal Matching Pursuit) and CoSaMP (Compressive Sampling Matching

Pursuit) optimization methods have been employed to solve the channel estimation problem [6] wherein underdetermined system of linear equations are solved under sparsity constraint. However, no compressive sensing *per se* has been carried out that targets shallow water acoustic channel with taking care of direct arrival, primary and secondary multipath consisting of both slow varying and rapid fluctuating components (shown in Fig. 1b) with varying degrees of sparsity of these components. Furthermore, non-uniform channel impulse response (i.e., delay spread) due to multipath arrivals in underwater acoustics communication provides background motivation to formulate the channel estimation problem in compressive sampling framework [6, 23, 25].

The confluence of adaptive signal processing, compressive sampling, and sparse recovery in the context of underwater acoustic communications is indeed encouraging and recently gained momentum in the shallow water acoustic communications literature [6, 7, 15, 20, 22, 23, 25].

Motivated with the above discussion, the objective of this research is to contribute to this momentum with a two-dimensional frequency-domain formulation of the underwater channel that complements existing formulations and enables robust localization of dominant components of the fundamentally non-stationary shallow water acoustic channel.

1.4 Contributions

Key contributions of this work can be summarized as below:

1. A two-dimensional frequency domain representation is obtained via carefully chosen transmitted signal design. This modeling transforms the problem of channel estimation to channel recovery in 2-D Fourier domain. Interestingly, this framework is similar to K-space based image reconstruction used in Magnetic Resonance Imaging (MRI) where CS is used extensively as default method for signal recovery. Similar to MRI domain, the underwater acoustic channel (vis-à-vis signal in MRI) is sparse in the 2-D Fourier domain. While the existing sparse recovery methods in UWA (Underwater Acoustic) channel estimation utilize sparseness of the channel in the time domain, the channel is sparser in the frequency domain. For example, refer to Fig. 1.3 that plots sorted magnitude of coefficients of the channel (of Fig.1.1) in the 2D time domain and the 2D frequency domain. It is observed that the sorted magnitude of coefficients of channel in the 2D frequency domain drops off more rapidly as compared to that of coefficients of channel in the 2D time domain and hence, the channel is sparser in the 2D Fourier domain. Thus, the proposed frequency domain representation allows CS framework to be inherited naturally. Here, it is pertinent to add that this framework has been proposed first time in UWA and is a significantly novel contribution of this work.

2. This work introduces non-uniform compressing sampling for shallow water acoustic communications. Specifically, techniques presented in this work perform random compressive sampling at different sampling rates across different frequency bands in the two-

dimensional frequency domain. Later in this work, it has been shown that simply using CS framework with basis pursuit denoising method does not yield good results because there is a need of detection of high-energy transients along with high-precision tracking of stationary but smaller delay taps. Thus, this work proposes non-uniform compressive sensing with prior information and non-uniform modified-CS [33] with prior information method for channel estimation wherein application domain knowledge is utilized with reference to frequency domain characteristics of the shallow water channel. Thus, this work illustrates the use of CS methods but by appropriately rooting them in this application domain. It should be noted that some of the existing methods use CS framework by setting up of problem as underdetermined system of linear equations under sparsity constraint [2, 6, 23]. However, non-uniform compressing sensing has not been used *per se* to shallow water acoustic channel estimation. In particular, we present non-uniform compressive sampling that is cognizant of the intricate interplay of multipath structure showing non-uniform structure with varying degrees of sparsity between slow-varying components and rapid fluctuations. This work actually uses compressively sensed data for channel recovery.

3. Extensive numerical validation of proposed techniques against existing techniques are provided based on channel estimates from field experiments as well as a public-domain channel simulator that has recently been tested against data from different field trials.

1.5 Organization, Notation and Units

This thesis is organized in six chapters. Chapter 2 presents details of experimental setup for ground truth on channel using channel estimates obtained from field experiments. Simulated channel is also discussed. In chapter 3, we present the mathematical formulation for the proposed alternative 2D Fourier domain representation of the channel with suitable transmitted signal design. We present the basic compressed sensing based channel reconstruction in chapter 4 with simulation results. Chapter 5 presents non-uniform compressed sensing frameworks for channel estimation using CS with prior information and modified-CS with prior information. This section presents results on SPACE08 channel data as well results on simulated channel from a recently proposed channel simulator in order to further substantiate the proposed work. Chapter 7 summarizes results of this work.

Notations: Lower case bold letters denote vectors, uppercase bold letters denote matrices, and lowercase italics letters denote scalars.

Units: Unless stated otherwise, delay taps are expressed as numerical indices with appropriate time windows stated in milliseconds and frequency units are given in Hz. Amplitude of the channel impulse response at a certain delay are interpreted in voltage units. This is because the delay taps are most directly reflective of a voltage at the A/D converter and can be related to uPa at the receiver through hydrophone specifications.

Chapter 2

Data for the Experiments

Numerical experiments presented in the work are based on channel taken from two independent sources. One is the real channel estimates from SPACE08 experiment and other is the simulated channel. These are described as follows.

2.1 Channel estimates from SPACE08 experiment

We use this channel estimate as the ground truth for testing the efficacy of the proposed method of channel estimation. Non-convex mixed norm solver (NCMNS) algorithm [2] is employed on experimental field data collected using BPSK-signalling in SPACE08 experiment conducted from October 18 to 27 in 2008 [1]. The wind and wave conditions varied substantially over this period. The channel was estimated approximately every 7.7 msecs duration using the above algorithm.

The SPACE08 experiment consisted of one transmitter and six receiving stations deployed at Martha's Vineyard Coastal Observatory (MVCO) and operated by Woods Hole Oceanographic Institution (WHOI). The experiment was conducted at shallow water depth of 15 m i.e. sea floor was at 15 m depth with transmitter and receiver at the sea floor. Receiving stations were fixed and also each receiving station was equipped with several hydrophones. Figure. 2.1 (taken from [1]) shows the setup of the experiment. Figure shows four stations labeled as S3, S4, S5 and S6. Stations S3 and S4 are 200 meters from the transmitter in the Southeast and Southwest directions, respectively. Stations S5 and S6 are 1000 meters from the transmitter in the Southeast and Southwest directions, respectively. In this work, we consider the channel estimated at the receiving stations which are at distance of 200 m from the transmitter. The seafloor at the experiment site was relatively flat and the temperature of the water column was constant.

The transmitted signals consisted of multiple repetitions of a 4095 point binary maximum length sequence transmitted at a symbol rate of 6.5 kbps and modulated at a central frequency of 11.5 kHz. A transmission three minutes in duration was made once every two hours. For

Figure 2.1: SPACE08 experiment setup

more details on the experimental setup, interested readers can refer to [1]. Figures 2.2 show channel estimates using [2], from the above mentioned experimental data, plotted as a function of time for 30 milliseconds duration collected over moderate to rough sea conditions.

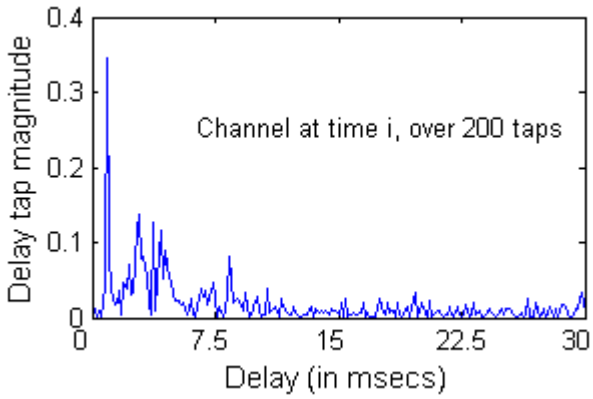

Figure 2.2: Representative channel estimates using [2] as kernel solver estimated from the field data of SPACE08 experiment [1]

2.2 Simulated channel

We also present results on a public-domain simulated channel that emulates multipath channel effects. This channel simulator has been proposed recently [3, 4] and is unrelated to channel estimates used in Section 2.1 above. This channel simulator models different multipath effects commonly encountered in shallow water acoustic communications, and has also successfully interpreted specular reflections and multipath arrivals in shallow water channel across several field trials [3, 4] including SPACE08 and other experimental channel data. Channel parameters used in this simulation work are presented in the Appendix. Impulse response of the simulated is shown in Figure. 2.3.

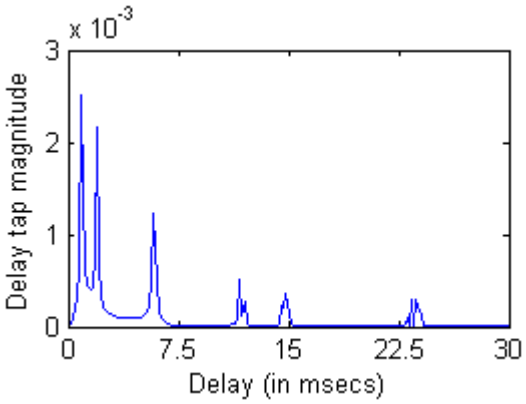

Figure 2.3: Channel impulse response simulated using public-domain simulator [3, 4]

Chapter 3

Dual Representation of the Channel in 2D Frequency Domain

We provide mathematical formulation for the alternative 2D representation of the channel impulse response in Fourier domain in this chapter. This is done by carefully choosing the transmitted signal design.

3.1 Notation used in the chapter

Following notations for channel parameters are introduced for the shallow water acoustic channel model, in addition to general notations discussed in Section 1.5

- K: Total number of delay taps;
- L: Total number of Doppler frequencies;
- i: time index;
- k: delay tap index, $k = 0, 1, \ldots, K$;
- l: Doppler frequency (dual domain to time dimension) index, $l = 0, 1, \ldots, L$;
- ω: delay frequency (dual domain to delay dimension) index, ω is quantized to same number of elements as delay taps, i.e., $\omega = 0, 1, \ldots, K-1$;
- $H[i,k], k = 1, \ldots, K$: Channel impulse response at time index i, measured at k^{th} delay tap; Thus, $\mathbf{H}$ denotes two-dimensional channel matrix in time-delay (i,k) domain;
- $\mathbf{U}$: Two-dimensional channel matrix in dual frequency or two dimensional frequency (l,ω) domain.

This section introduces a non-uniform compressive sampling and sparse recovery scheme that exploits the separation of non-sparse structure at low frequencies and the sparse structure

at higher frequencies in the two-dimensional frequency representation presented in the sequel (refer to (3.4)).

3.2 Mathematical formulation for 2D Fourier domain representation of the channel

The key idea behind the mathematical formulation is that transmitted signals will be constructed as an orthogonal basis in (l, ω) domain, thus reducing the channel estimation problem to spectral sampling problem in the two-dimensional Fourier domain. Consider complex exponential input signal $x[i, \omega] = e^{j\frac{2\pi i\omega}{K}}$, corresponding to delay frequencies $\omega = 0, 1, \ldots, K-1$ across parallel K no. of sub-channels. These K sub-channels may be easily designed in baseband using appropriate frequency selective techniques. In addition, consider L Doppler frequencies $l = 0, 1, \ldots, L-1$ for sampling the channel in the Doppler domain. On transmission of the above designed input signal over the time-varying K-length channel impulse response $H[i, k]$, one obtains

$$\begin{aligned} y[i, \omega] &= \sum_{k=0}^{K-1} H[i, k] x[i-k, \omega] \\ &= \sum_{k=0}^{K-1} H[i, k] e^{j\frac{2\pi(i-k)\omega}{K}} \\ &= e^{j\frac{2\pi i\omega}{K}} \sum_{k=0}^{K-1} H[i, k] e^{-j\frac{2\pi k\omega}{K}}. \end{aligned} \tag{3.1}$$

On multiplying both sides of (3.1) with $e^{-j\frac{2\pi i\omega}{K}}$, one obtains

$$y[i, \omega] e^{-j\frac{2\pi i\omega}{K}} = \sum_{k=0}^{K-1} H[i, k] e^{-j\frac{2\pi i\omega}{K}}. \tag{3.2}$$

On computing the one-dimensional Fourier transform of the time variable i in (3.2), that corresponds to Doppler frequency, one obtains

$$\begin{aligned} U[l, \omega] &= \sum_{i=0}^{L-1} y[i, \omega] e^{-j\frac{2\pi i\omega}{K}} e^{-j\frac{2\pi il}{L}} \\ &= \sum_{i=0}^{L-1} \sum_{k=0}^{K-1} H[i, k] e^{-j\frac{2\pi k\omega}{K}} e^{-j\frac{2\pi il}{L}}, \end{aligned} \tag{3.3}$$

where (3.3) represents 2-D Fourier transform of the channel impulse response $H[i, k]$, $\omega = 0, 1, 2, \ldots, K-1$ and $l = 0, 1, 2, \ldots, L-1$. Equation (3.3) can be re-written as

$$\mathbf{U} = \mathbf{F}_1 \mathbf{H} \mathbf{F}_2 = \mathfrak{F}\mathbf{H}, \tag{3.4}$$

where $\mathbf{U}$ is the matrix form of $U[l, \omega]$ of size $L \times K$, $\mathbf{H}$ is the matrix form of channel impulse response $H[i, k]$ of size $L \times K$, $\mathbf{F}_1$ is the $L \times L$ Fourier transform matrix, $\mathbf{F}_2$ is the $K \times K$ Fourier transform matrix, and $\mathfrak{F}$ is the symbolic notation of 2-D Fourier transform operator.

The above formulation clearly shows that perfect channel recovery can be done in noise free scenario via two-dimensional inverse Fourier transform of the post-processed received signal $\mathbf{U}$. Thus, designing the transmitted signal and post-processing the received signal in the two-dimensional (ω, l) domain has transformed the problem of channel estimation in time-domain to channel recovery from its salient spectral features: both along delay frequency dimension ω, signifying channel micro-structure, and the Doppler frequency dimension l, signifying fast or slowly varying trends. As discussed in the sequel, the support of these channel features, while exhibiting high spikes against the background, varies significantly between low and high Doppler frequencies, thus motivating the case for non-uniform compressive sampling in the 2D frequency domain.

Interestingly, the proposed framework is similar to k-space based image reconstruction in Magnetic Resonance Imaging (MRI) [34, 35] where images are captured in 2D Fourier domain instead of the spatial domain. Compressive Sensing (CS) is extensively used approach for image reconstruction in MRI where few 2D Fourier transform samples of MRI images are sensed for full spatial domain image reconstruction. This motivates us to explore CS approach in the proposed framework where full channel, $\mathbf{H}$ is recovered from partial samples of post-processed received signal $\mathbf{U}$. This is described in next chapter. We further extend CS approach in chapter 5 to employ non-uniform partial sampling on $\mathbf{U}$ and use prior information about the channel for its full recovery. This is to note that the above proposed formulation is a completely new way of presenting channel estimation problem.

3.3 Justification for two-dimensional Fourier representation

A snapshot of 2-D Fourier transform or Fourier dual of delay spread and time is illustrated in Fig. 3.1. It is noteworthy that the two-dimensional frequency representation shows clusters of slowly varying channel components across the low Doppler frequencies, while *variability along the impulse response structure of these slowly varying channel components are recorded along the ω axis*. The transient channel components are recorded along the higher Doppler frequencies. Key benefits behind this representation are three-fold:

(i) Channel microstructure specific to slowly varying channel components gets highlighted along the ω (delay-frequency) axis; this allows high-precision recovery of these components, which are critical to effective underwater communication systems;

(ii) Slow-varying channel components, localized in lower Doppler frequencies, are easily disambiguated against rapidly fluctuating channel components localized in higher Doppler frequencies; and

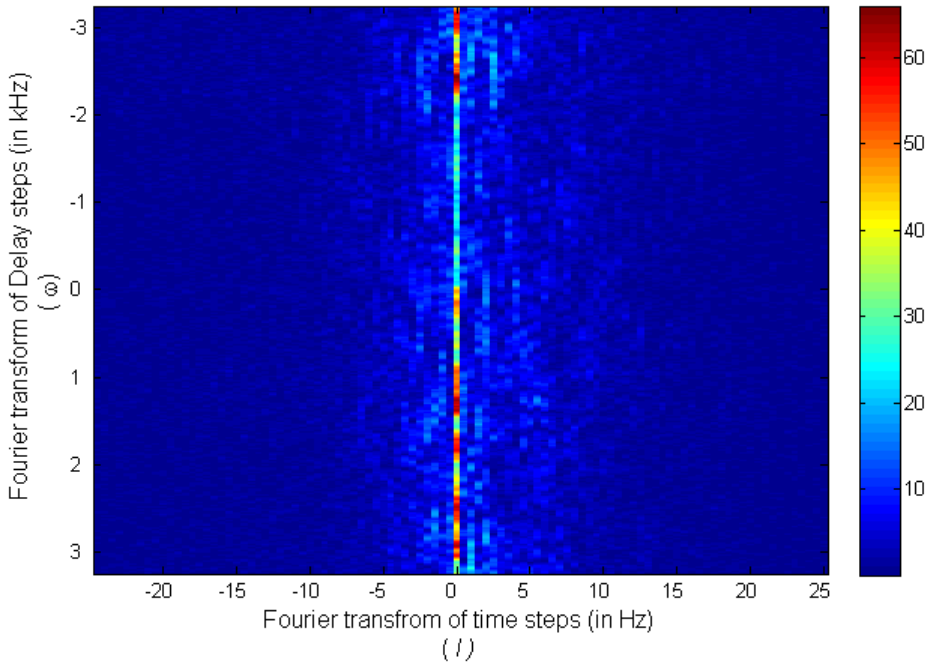

Figure 3.1: 2-D Fourier Transform of channel in baseband (estimated from field data of SPACE08 experiment [1]) shown in Fig. 1.1; Note: Colorbar is linear.

(iii) This representation allows a non-uniform compressive sampling framework, where the slowly-varying components in the lower Doppler frequencies occupy a significantly broader support than the high-energy channel transients along the higher Doppler frequencies.

Chapter 4

Channel Estimation using Basic Compressive Sensing Techniques

As discussed in previous chapter, formulation (3.4) clearly shows that perfect channel recovery can be done in noise free scenario via two-dimensional inverse Fourier transform of the post-processed received signal $\mathbf{U}$. In general, the received underwater acoustic signal will be corrupted with noise. This chapter presents the channel estimation problem in compressed sensing framework with noisy channel scenario.

4.1 Channel estimation in noisy scenario

With the mathematical formulation, given in the previous chapter, we have transformed the channel estimation problem to channel recovery in 2D Fourier domain. In case of noisy scenario, this formulation transforms channel estimation problem to denoising based channel recovery in the 2-D Fourier domain. Since additive white Gaussian noise (AWGN) will remain AWGN under any orthogonal transformation, it will remain AWGN under Fourier transform of the received signal in (3.3). Thus, (3.4) can be re-written in the presence of noise as below:

$$\mathbf{U}_n = \mathfrak{F}\mathbf{H} + \mathbf{N}, \tag{4.1}$$

where $\mathbf{U}_n$ is the noisy version of $\mathbf{U}$ and $\mathbf{N}$ is the complex white Gaussian noise matrix. Since channel $\mathbf{H}$ is known to be sparse in the underwater communication literature [2,7], the problem can be formulated as BPDN (Basis Pursuit Denoising) problem [36] and is, mathematically, given by

$$\underset{\mathbf{H}}{min}||\mathbf{H}||_1 \quad \text{subject to } ||\mathbf{U}_n - \mathfrak{F}\mathbf{H}||_2^2 \leq \epsilon, \tag{4.2}$$

where $||\mathbf{V}||_1$ denotes sum of the absolute values of $\mathbf{V}$, $||\mathbf{V}||_2^2$ denotes sum of the squares of the values of $\mathbf{V}$ and ϵ is the measure of the noise in post-processed received signal.

Equivalently, the problem can also be modeled mathematically as

$$\min_{\mathbf{H}} ||\mathbf{U}_n - \mathfrak{F}\mathbf{H}||_2^2 \quad \text{subject to } ||\mathbf{H}||_1 \leq \tau. \tag{4.3}$$

The above formulation is termed as LASSO (Least Absolute Shrinkage and Selection Operator) [29] and τ is the measure of the sparsity of the channel $\mathbf{H}$.

While (4.2) or (4.3) can be solved for underwater acoustic channel estimation in noisy scenario, we explore compressed sensing based approach for the same based on the discussion in section 3.2. This is explained in next section.

4.2 Partial Fourier Sampling Based Channel Estimation- Basic CS

In this section, we present compresseived sensing based channel estimation from it's 2D Fourier domain representation. Consider the compressively sensed version of $\mathbf{U}$ (2D Fourier representation of the channel) as below:

$$\mathbf{U}_{sub} = \mathfrak{R}\mathfrak{F}\mathbf{H} + \mathbf{N}, \tag{4.4}$$

where $\mathbf{U}_{sub}$ is the compressively-sampled and noisy measurement of $\mathbf{U}$ and $\mathfrak{R}$ is the random binary sub-sampling operator or a matrix consisting of '1's and '0's that allows random selection of positions in 2-D Fourier domain leading to different sampling ratios. $S\%$ sampling ratio implies $\lfloor \frac{LK \times S}{100} \rfloor$ number of samples are being captured randomly from the full post-processed signal $\mathbf{U}$. The channel recovery in denoising-based basic CS framework can be formulated as

$$\min_{\mathbf{H}} ||\mathbf{U}_{sub} - \mathfrak{R}\mathfrak{F}\mathbf{H}||_2^2 \quad \text{subject to } ||\mathbf{H}||_1 \leq \tau. \tag{4.5}$$

Interestingly, it is noticed from Figures 1.2 and 1.3 that the two-dimensional Fourier transform of channel, i.e., $\mathfrak{F}\mathbf{H}$ is more sparse than the channel itself. Thus, it is proposed to estimate channel $\mathbf{H}$ in the CS based denoising framework considering the sparsity of $\mathbf{U}$ as below:

$$\min_{\mathbf{U}} ||\mathbf{U}_{sub} - \mathfrak{R}\mathbf{U}||_2^2 \quad \text{subject to } ||\mathbf{U}||_1 \leq \tau, \tag{4.6}$$

where $\mathbf{U} = \mathfrak{F}\mathbf{H}$ and τ is the measure of the sparsity of $\mathbf{U}$.

In the following experiments, the value of τ is set to $0.5\sqrt{LK}$, where L is the granularity of Doppler frequencies and K is the number of delay frequencies. This value of τ is found to provide good estimate of channel in all the experiments presented in this work and is found empirically. Fig. 4.1 shows the channel reconstruction accuracy in terms of NMSE as a function of c, where $\tau = c\sqrt{LK}$ keeping all other parameters (sampling ratio, window length, no. of delay taps) fixed. The experiment is carried out at 70% sampling ratio at noisy channel SNR of 5 dB

for three window length, 7.68 msecs, 9.22 msecs and 10.75 msecs. The plot is shown to illustrate change in channel accuracy with τ/c and hence, this allows us to select an optimal value of τ/c. The figure shows that NMSE is reasonably low with $c = 0.5$ or when $\tau = 0.5\sqrt{LK}$ for all the three window length. In addition, this value worked for all sampling ratios and hence, is used in all experiments (and at all sampling ratios) presented in this work. It should be noted that there is no relation between sampling ratio and τ/c. They are independent of each other.

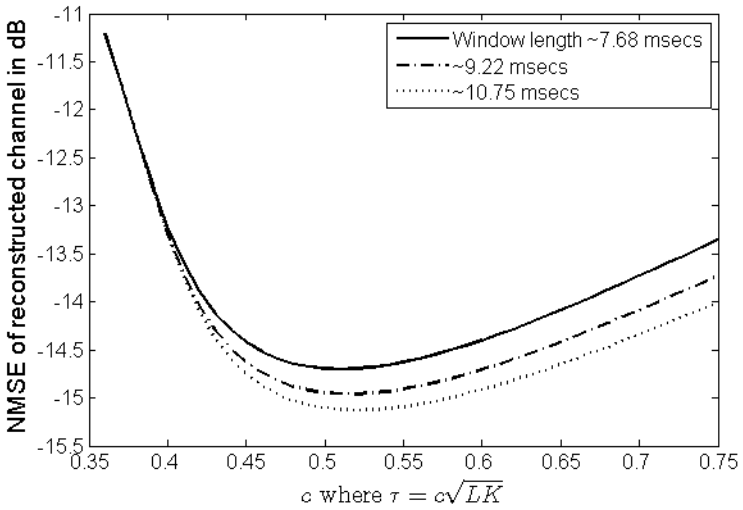

Figure 4.1: Reconstruction accuracy of channel in terms of NMSE versus the value of c where $\tau = c\sqrt{LK}$

The problem has been solved with the MATLAB toolbox SPGL1 [37, 38].

In order to test the performance of the proposed channel estimation method with basic CS, Monte Carlo simulations are carried out over 200 iterations for each noise level. The performance is evaluated via normalized mean squared error (NMSE) measured in decibels (dB). Results are displayed over additive white complex Gaussian noise of varying variance. In addition, different window lengths are considered for channel estimation. The signal-to-noise ratio (SNR) of noisy channel is computed as below:

$$\text{SNR of Noisy Channel} = 10\log_{10}\left(\frac{\frac{1}{LK}\sum_{i=0}^{L-1}\sum_{k=0}^{K-1}|H(i,k)|^2}{\sigma_n^2}\right), \tag{4.7}$$

where σ_n^2 represents the noise variance.

The normalized mean squared error (NMSE) of estimated channel $\hat{H}[i,k]$ measured in dB

is computed as below:

$$\text{NMSE} = 10\log_{10}\left(\frac{\sum_{i=0}^{L-1}\sum_{k=0}^{K-1}|H(i,k)-\hat{H}(i,k)|}{\sum_{i=0}^{L-1}\sum_{k=0}^{K-1}|H(i,k)|^2}\right). \tag{4.8}$$

Fig. 4.2 and 4.3 represent NMSE results on channel recovery using basic CS approach given in (4.6). Corresponding to CS, impact of varying sampling percentage in the two-dimensional Fourier domain on channel recovery is studied. As SNR decreases from 10 dB to 5dB, an increase in NMSE is observed with most pronounced increase ($\sim$ 3dB) at 100% sampling ratio. Further, it is observed that sampling ratio increase leads to progressively superior performance, with lowest NMSE attained at 100% (i.e. no compressive sampling that is actually *sparsity-constraint least squares*). Thus, it is concluded that traditional compressive sampling as used in (4.6) does not lead to good channel recovery.

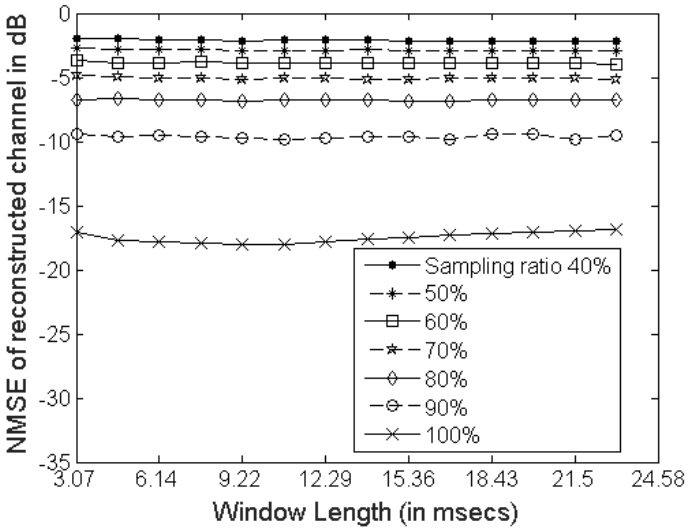

Figure 4.2: NMSE results on channel estimation using the traditional CS at noisy channel SNR of 10dB; implements (4.6).

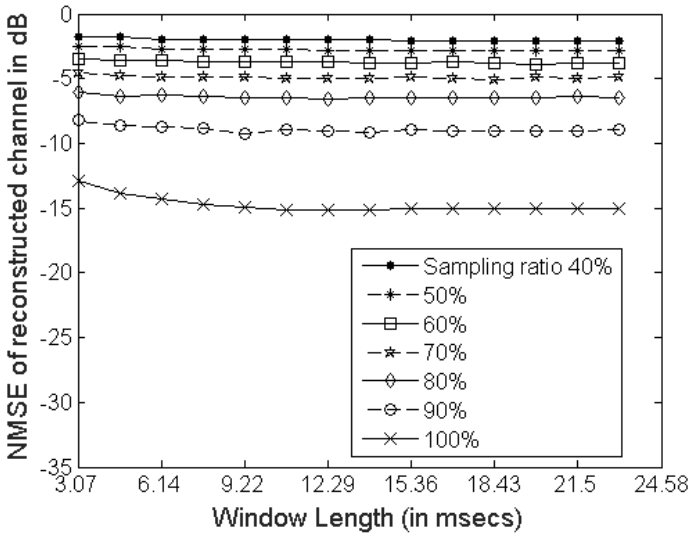

Figure 4.3: NMSE results on channel estimation using the traditional CS at noisy channel SNR of 5dB; implements (4.6).

Chapter 5

Channel Estimation using Compressed Sensing with Prior Information

We reached at the conclusion at the end of the previous chapter that using compressed sensing only does not lead to good channel estimation specially at lower sampling ratio. We also discussed in 3.3 that the 2D Fourier domain representation of the channel is cognizant of slow and rapidly fluctuating channel components. Also, dominant components of the channel lie at the low Doppler frequency whereas highly fluctuating components which constitute less energy lie at higher Doppler frequencies. This motivates us to use non-uniform compressed sensing to reconstruct the channel, heavily sampling lower Doppler frequencies and sampling higher Doppler frequencies at lower sampling rate. This is described in following sections.

5.1 Proposed Channel Estimation using Compressive Sensing with Prior Information

Consider the following observations from Figures 1.1 to 1.2:

1. Direct arrival and primary multipath regions dominate the channel support (Fig. 1.1- 1.2).
2. The zero Doppler frequency column $\mathbf{U}[0,\omega]_{\omega=0}^{K-1}$, in Fig. 1.2 is the most dominant component of the channel. Physically, it represents the time-invariant slowly changing component due to direct arrival and persistent multipath arrivals.
3. Rest of the support $\mathbf{U}[l\neq 0,\omega]_{l=1,\omega=0}^{L-1,K-1}$ is dominated by slower Doppler frequency components, particularly, $\mathbf{U}[\pm 1,\omega]_{\omega=0}^{K-1}$.
4. Rapidly fluctuating multipath arrivals (observed in higher numbered delay taps in Fig. 2.2) occupy high-frequency columns of $\mathbf{U}[l\neq 0,\omega]_{l=2,\omega=0}^{L-1,K-1}$ as high-energy components, i.e., for

$l \geq 2$.

The above observations imply co-existence of dominant slowly varying component and high-energy transients. All the above observations are based on the 2D frequency domain representation of the channel proposed in this work via carefully chosen transmitted signal design and this framework has been proposed for the first time in underwater acoustic communication. As per our knowledge, the four observations made above are not being explicitly used in other works and thus, current sparse sensing literature [26–28] as well as the proposed framework in previous chapter ignores these physical constraints posed on $\mathbf{U}[l,\omega]_{l=0,\omega=0}^{L-1,K-1}$ due to multipath propagation in the shallow water acoustic paradigm.

It should be noted that, although above observations are based on SPACE08 experiment channel estimates, these observations hold in general depending on the state of the ocean. If the ocean is very calm and there are no other disturbances, the low Doppler activity may dominate till 5 Hz and there is hardly any activity in high Doppler frequencies. If the ocean is very rough with high wind and other (like motion of ship and ocean animals) activities, significant surface wave reflections may push the dominated low Doppler boundaries to higher frequency range.

The observations made above establish motivation for employing acoustic physics-cognizant * channel knowledge to densely sample in the zero- and low- Doppler frequency regions that correspond to dominant oceanographic activity. This proposed framework is hereby, called as non-uniform compressive sensing with prior knowledge.

In order to formulate it mathematically, assume that T denotes the support of $\mathbf{U}$ that contains dominant slowly varying components of the channel. All samples on the support T are considered and partial sensing is carried out on $|T^c| = n - |T|$, where $|.|$ denotes the cardinality of a set and n denotes the number of elements of $\mathbf{U}$. Subsequently, channel $\mathbf{H}$ is estimated in CS with prior information based denoising framework as below:

$$\min_{\mathbf{U}} ||\mathbf{U}_{sub} - \mathfrak{R}_{T^c}\mathbf{U}||_2^2 \quad \text{subject to } ||\mathbf{U}||_1 \leq \tau, \tag{5.1}$$

where $\mathbf{U} = \mathfrak{F}\mathbf{H}$ and $\mathfrak{R}_{T^c}$ denotes restricted sampling operator that does partial sensing on T^c. Hence, $S\%$ sampling ratio implies $\lfloor \frac{LK \times S}{100} \rfloor$ samples are to be captured from the whole post-processed received signal $\mathbf{U}$, out of which $|T|$ number of samples belong to support T as it is fully sampled and rest of the samples i.e. $\lfloor \frac{LK \times S}{100} \rfloor - |T|$ number of samples are randomly captured from the support T^c.

*We call physics-cognizant because physics based phenomena such as surface wave focusing and specular reflections have been duly considered in this work. Surface wave focusing are sparsely distributed in delay spread and may occupy both primary as well as secondary multipath bands whereas specular reflections occupy primary multipath bands. Surface focusing events occupy high Doppler frequencies being present sparsely and specular reflections occupy low Doppler frequencies because of their slow varying nature.

5.1.1 Frequency-selective noise suppression using CS with prior information

Sparse recovery using (5.1) differs from the traditional CS formulation (4.6) in two significant ways:

a. Sparse recovery is imposed on the entire space, i.e., the solution is heavily biased towards picking the highest components of the channel across the whole support.

b. Partial sampling is limited to outside the main support.

In order to test bullet point 'b' above, results are presented on SPACE08 channel with no partial sampling or full sampling of zero Doppler in Fig. 5.1 and 5.2 (with noisy channel SNR of 10 dB and 5 dB respectively) and, full sampling of zero Doppler plus first one low and first two low Doppler frequency columns in Fig. 5.3 and 5.4 respectively at noisy channel SNR of 5 dB. The combination of these two criteria biases the channel recovery solution in (5.1) towards selecting the frequency channel components belonging to main support of the channel, e.g., in this case the zero and low Doppler frequency components. This is partly due to the dominance of these components over the rest of the support as well as noise averaging over the lower frequency components, relative to higher frequency transients. Therefore, channel components in higher frequency region represented by outer columns experience lower SNR compared to channel components in inner columns due to different rates of noise averaging. This leads to frequency-selective noise suppression using sparse recovery techniques along the l axis. It is noteworthy that the exact choice of what constitutes low Doppler depends on the state of the ocean, e.g., for really rough ocean with high wind activity, significant surface wave phenomena can push the choice of low Doppler boundaries [5-10Hz] to higher ranges.

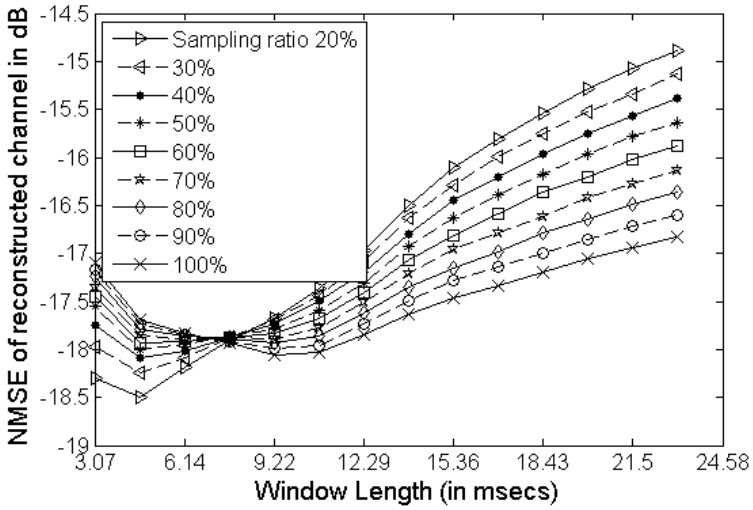

Figure 5.1: NMSE results on channel estimation using CS with prior information, i.e., with full sampling of **zero Doppler frequency**; with noisy channel SNR=10dB; implements (5.1).

For the experimental SPACE08 field data used in this Section, limiting Doppler activity observations to only ± 1 column next to zero Doppler was sufficient for capturing most multipath

activity leaving outer columns for high-transient observations. The low-Doppler region of the channel is notated as $U[|l| \leq \theta, \omega]_{l=0,\omega=0}^{\theta,K-1}$, where θ is the chosen upper bound of the low Doppler frequency range. Choosing $\mathfrak{R}_{T^c}$ with a smaller sampling ratio will select all the dominant low-frequency activity around $U[|l| \leq \theta, \omega]_{l=0,\omega=0}^{\theta,K-1}$ and select only some of the high-energy component from the rest of the support.

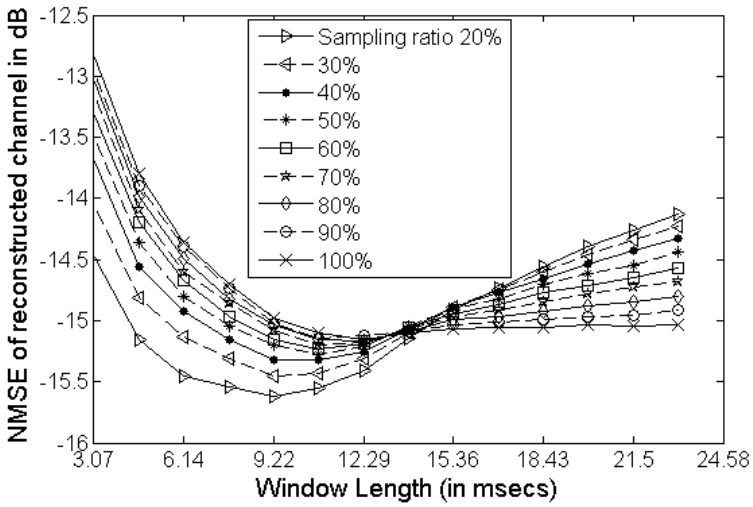

Figure 5.2: NMSE results on channel estimation using CS with prior information, i.e., with full sampling of **zero Doppler frequency**; with noisy channel SNR=5dB; implements (5.1).

NMSE results on channel estimation are presented considering full sampling in

a. zero Doppler frequency region of **U** at 10dB (Fig. 5.1) and 5dB (Fig. 5.2) of noisy channel SNR,

b. zero Doppler and first (± 1) column adjacent to zero Doppler at 5dB noisy channel SNR (Fig. 5.3), and

c. zero Doppler and first two columns (± 2) adjacent to zero Doppler components at 5dB noisy channel SNR (Fig. 5.4).

In Fig. 5.1-5.4, a clear minimum error is observed for each sampling ratio, even though the minimum may be achieved over different observation windows. This is due to the inherent uncertainty principle governing time, frequency, and sparsity localization, discussed in [10]. The minimum is achieved when the observation window is long enough to capture $U[0, \omega]_{\omega=0}^{K-1}$, i.e., the zero-Doppler column precisely, for the given sampling ratio. Beyond this point, increasing the observation window length will not add to the precision of detecting $U[0, \omega]_{\omega=0}^{K-1}$ but may reduce the precision of estimating higher Doppler columns, as high-energy transients may get averaged over longer window choices.

Further discussion of results regarding relative performance between different sampling ratios are given below.

5.1.2 Understanding NMSE behavior with different sampling ratios

In order to further understand NMSE results on channel estimation using CS with prior information, the performance of Fig. 5.1 and 5.2 are compared with those of Fig. 4.2 and 4.3 for noisy channel SNR=10dB and 5dB, respectively. Significantly improved performance is observed over the traditional basic CS. This is to be expected as (4.6) is agnostic of channel support and blindly attempts recovery of the channel based on sparsity defined randomly over the whole space. On the other hand, (5.1) assumes basic physical knowledge of the channel support and therefore, samples it more efficiently.

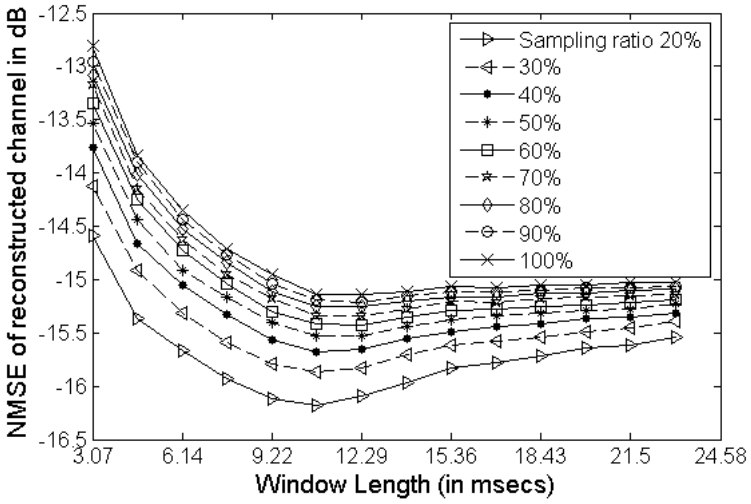

Figure 5.3: NMSE results on channel estimation using CS with prior information, i.e., with full sampling of **zero- and first low-Doppler frequency**; with noisy channel SNR=5dB; implements (5.1).

Further, it is observed that NMSE converges across all sampling ratios to a cross-over point in Fig. 5.1 and 5.2 as observation window increases followed by a reversal in performance across the sampling ratios in terms of NMSE performance. This is attributed to the NMSE (5.2) being dominated by the error in estimating the zero-Doppler column $U[0,\omega]_{\omega=0}^{K-1}$, as demonstrated by Tables 1 and 2.

$$\text{NMSE(in dB)} = 10\log_{10}\left(\frac{\sum_{\omega=0}^{K-1}|U(i,\omega)-\hat{U}(i,\omega)|^2}{\sum_{\omega=0}^{K-1}|U(i,\omega)|^2}\right), \tag{5.2}$$

where i corresponds to

a. column (a) in Tables 1 and 2 — zero Doppler or the center column of Fig. 1.2,

b. column (b) in Tables 1 and 2 — squared sum of errors in the I column to the left and right of the center column (zero Doppler) of Fig. 1.2, and

c. column (c) in Tables 1 and 2 — squared sum of errors in the II column to the left and right of the center column (zero Doppler) of Fig. 1.2.

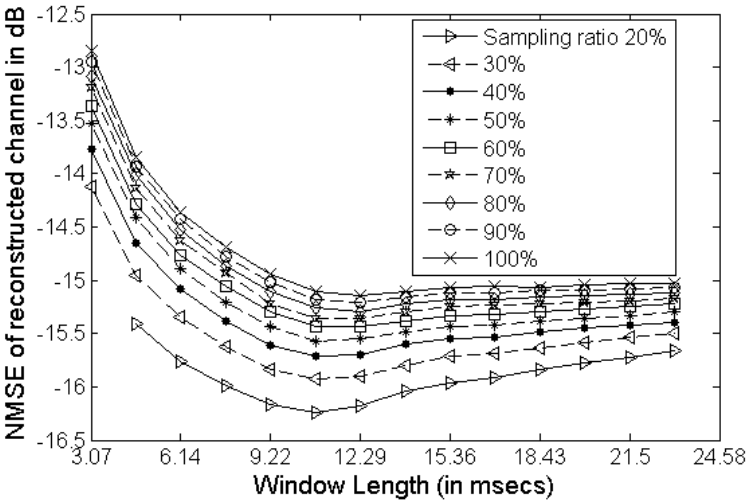

Figure 5.4: NMSE results on channel estimation using CS with prior information, i.e., with full sampling of **zero- and first two low-Doppler frequencies**; noisy channel SNR=5dB; implements (5.1).

Channel recovery with the smallest sampling ratio (40%) recovers the zero-Doppler column $U[0,\omega]_{\omega=0}^{K-1}$ fastest, due to heavy noise suppression along the higher Doppler columns (section 5.1.1), whereas higher sampling ratios need to observe the channel longer to resolve noise suppression. This is further evidenced by the shift in the cross-over point from approx. 7 milliseconds in Fig. 5.1 to approx. 13 milliseconds in Fig. 5.2 as the SNR is decreased from 10 dB to 5 dB.

Fig. 5.3 and 5.4 correspond to full sampling of zero and first Doppler columns, i.e., $U[|l| \leq 1,\omega]_{l=0,\omega=0}^{1,K-1}$ (Fig. 5.3) and zero Doppler and first two Doppler columns, i.e., $U[|l| \leq 2,\omega]_{l=0,\omega=0}^{2,K-1}$ (Fig. 5.4). Fig. 5.3 and 5.4 do not display significant difference because activity from second Doppler column, i.e., $U[|l| = 2,\omega]_{\omega=0}^{K-1}$ is not that significant relative to energy in $U[0,\omega]_{\omega=0}^{K-1}$. Both figures exhibit progressively lower NMSE for smaller sampling ratios, without any cross-over point like in Fig. 5.1 and 5.2. This is to be expected, as all estimators in both figures sample the lower Doppler columns, i.e., $U[|l| \leq \theta,\omega]_{l=0,\omega=0}^{\theta,K-1}$ with 100% sampling ratio ($\theta = 1$ for Fig. 5.3 and $\theta = 2$ for Fig. 5.4). In Fig. 5.3 and Fig. 5.4, sampling ratios differ only across higher Doppler frequency columns that capture high-energy transients and other ephemeral events. Thus, both these figures demonstrate similar performance in channel estimation. The difference in performance across different sampling ratios as well as between corresponding curves in Fig. 5.3 and 5.4 depend only on the ability of the algorithm to pick up transient multipath energy at higher frequencies. The lower sampling ratios are heavily biased towards capturing only the high-energy transients in this domain due to their superior noise suppression and hence, achieve lower NMSE than higher sampling ratios. Furthermore, higher energy transients average out with increasing window length, and hence, the performances of all estimators deteriorate

after achieving minimal NMSE point at approx. 10.8 milliseconds.

The above analysis shows that one needs to choose appropriate window length and appropriate sampling ratio in order to perform channel estimation. From Figures 5.3 and 5.4, it is observed that when the observation window is long enough to capture slowly varying components, the performance of the method stabilizes, i.e., increasing the window length beyond, say, 9.22 msec does not change performance much. Figure-5.5 shows NMSE vs noisy channel SNR for window length from 6.14msecs to 15.36msecs using CS with prior information i.e. with full sampling of zero- and first two low-Doppler frequency and overall sampling ratio of 70%. It is observed that curves of different window lengths run almost together between nearly 5-10dB of noisy channel SNR. Thus, any window length between 9.22msec to 15.36msec is appropriate to provide good performance at these SNRs.

Fig. 5.6 shows the variation of NMSE versus sampling ratio at noisy channel SNR of 5dB (corresponding to Fig. 5.4) to carefully look at the impact of sampling ratio on NMSE at different window lengths. It is observed that at 5dB channel SNR, window lengths from 10.75 to 23.04 msec provide almost consistent performance from 60% sampling ratio onwards (with an NMSE change within $\pm$0.5dB). Better performance is observed at lower sampling ratios with an improvement of 0.5dB to 0.8dB compared to 100% sampling ratio because the channel is sparse in the 2D frequency domain where the proposed CS based method is applied. Also, since the channel SNR is low (5dB), channel is noisy and hence, lower sampling ratio will help in picking less but higher energy transients that are more likely to be higher SNR points in the frequency domain.

5.1.3 Adaptive approach to selecting observation window length and sampling ratio

An adaptive approach similar to [20] is presented for appropriate selection of observation window length and sampling ratio that minimizes the normalized prediction error. The approach is described in steps as follows:

a. Step 1: Initialize window length and sampling ratio at some point, called the current operating point.

b. Step 2: Choose window length on either side of the current operating point. If the prediction error decreases, go until the optimum point is reached.

c. Step 3: Choose the sampling ratio on either side of the current setting and move in the direction of decrease of NMSE and choose the one with minimum NMSE.

In real setting, training signal can be sent from the transmitter to the receiver which is already known there. Normalized prediction error in that case can be estimated over that training signal and the above approach can be used to find the appropriate window length and sampling ratio that minimizes this normalized prediction error.

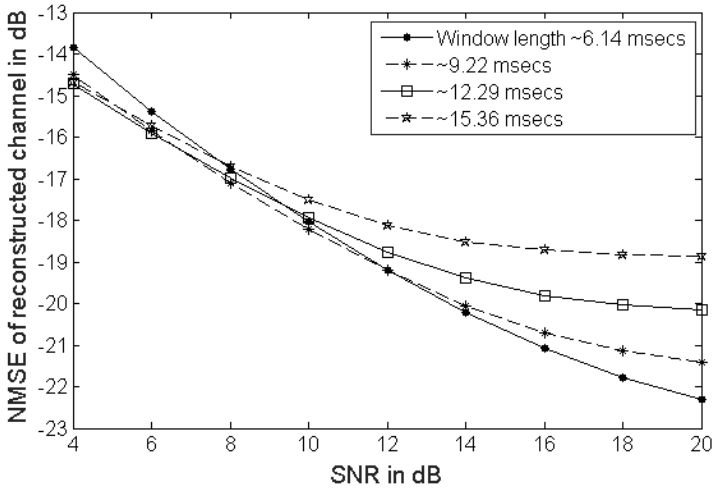

Figure 5.5: NMSE vs noisy channel SNR using CS with prior information i.e. with full sampling of **zero- and first two low-Doppler frequency** and with 70% sampling ratio; at different window lengths

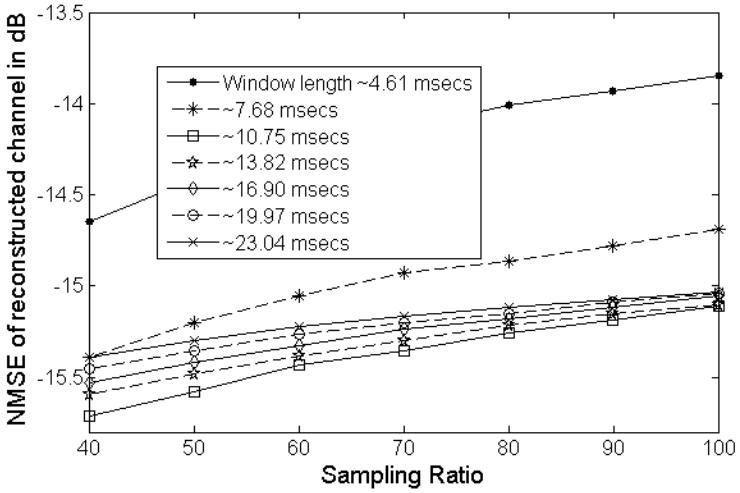

Figure 5.6: Perturbation analysis for the case when full sampling is done of **zero- and first two low-Doppler frequency** with noisy channel SNR=5dB (i.e. corresponding to Fig. 5.4)

5.2 Proposed Channel Estimation using *Modified* CS with Prior Information

Previous subsection utilized non-uniform CS with prior information. In addition to the observations made in the previous subsection, it can be noted from Fig. 1.2 that Fourier transform of the channel $\mathbf{U}$ is sparser on the support T^c rather than the entire support (refer to Figure-5.7). So, imposing the sparsity of $\mathbf{U}$ on T^c, unlike (5.1) that imposes sparsity on the entire support of $\mathbf{U}$, can increase the performance of channel estimation. This can be easily formulated in the context of modified CS [33]. Here, non-uniform modified CS with full sampling of zero Doppler frequency component of the channel transform $\mathbf{U}$ is utilized. In specific, the support of $\mathbf{U}$ is

split into two non-overlapping subspaces S_1 and S_2:

a. Subspace S_1 corresponds to support T^c where sparsity is imposed and partial sampling is carried out. This subspace is noisy and sparse, and corresponds to multiple reflections between the ocean surface and rough sea bottom, transient signal spikes from unpredictable wave focusing events and low energy fluctuations due to attenuated multipath arrivals.

b. Subspace S_2, the less noisy subspace complementary to (i) above, i.e., support T, where neither partial sampling is done nor sparsity is imposed. This subspace corresponds to relatively stable and higher-energy components that occupy the low-Doppler regions.

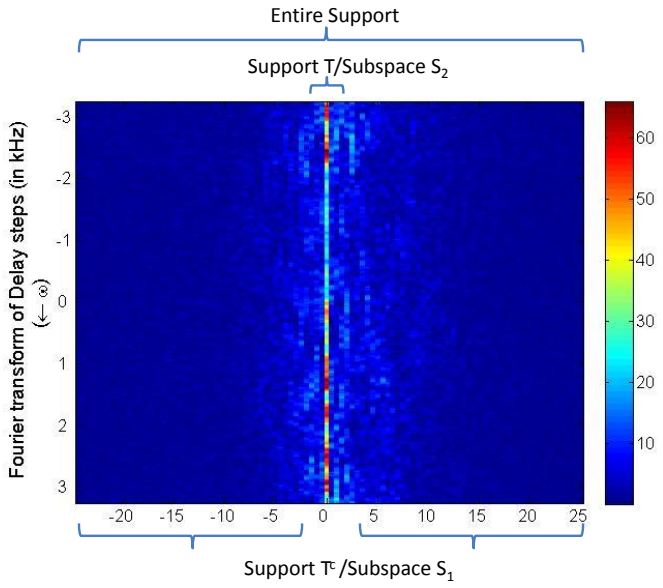

Figure 5.7: 2D Fourier representation of channel with labeling of subspaces and support

The proposed modified CS with prior information framework is now formulated as below

$$\min_{\mathbf{U}} ||\mathbf{U}_{sub} - \mathfrak{R}_{T^c}\mathbf{U}||_2^2 \quad \text{subject to } ||\mathbf{U}_{T^c}||_1 \leq \tau, \tag{5.3}$$

where $\mathbf{U} = \mathfrak{F}\mathbf{H}$ and $\mathfrak{R}_{T^c}$ is the restricted sampling operator that does partial sensing on T^c. Channel estimation results are presented using the modified CS approach considering support T to be zero Doppler frequency region of $\mathbf{U}$ at 10dB (Fig. 5.8) and 5dB (Fig. 5.9) of noisy channel SNR.

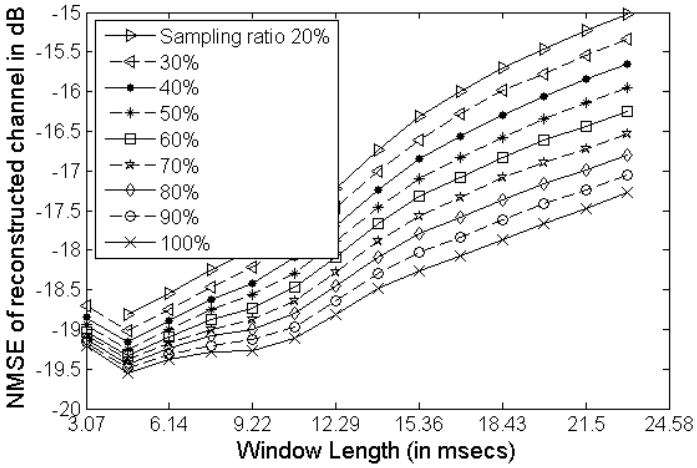

Figure 5.8: NMSE results on channel estimation at 10dB SNR with **modified CS**, support T is **zero Doppler frequency**; implements (5.3).

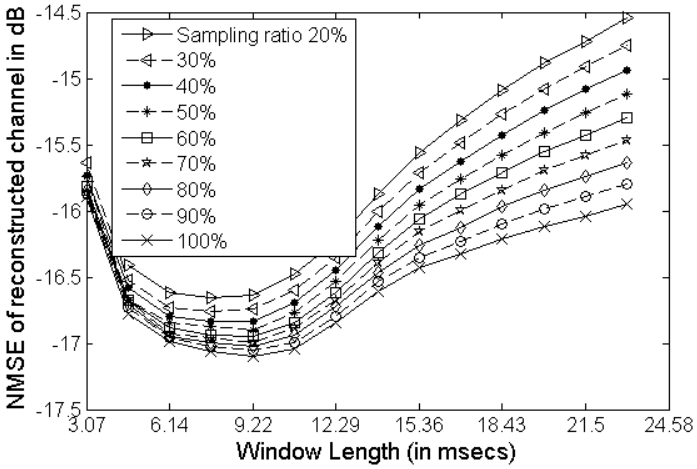

Figure 5.9: NMSE results on channel estimation at 5dB SNR with **modified CS**, support T is **zero Doppler frequency**; implements (5.3).

5.2.1 Discussion of Results

Fig. 5.8 and 5.9 present NMSE results with *modified CS with prior information* as given in (5.3) and reveal that lower NMSE is achieved with 100% sampling ratio compared to 40% sampling ratio. This is to be expected as the contribution of the high-energy regions in the low-Doppler frequency space S_2 is explicitly accounted for in the sparsity and partial sampling considerations in (5.3), unlike (5.1). Thus, due to explicit prior setting in (5.3) lower sampling ratios do not offer any bias towards estimating the high-energy low-Doppler components. Furthermore, the partial sampling operator $\mathfrak{R}_{T^c}$ only captures sparsity in S_1 while suppressing background noise. Also, these results are in consonance with compressive sensing theory, whereby, 100% sampling ratio provides the lowest NMSE and NMSE increases with decreasing sampling ratio [39, 40].

5.3 Comparative Results

In this subsection, comparative results on channel estimation are presented with direct denoising based framework, i.e., least squares with sparsity regularization [41], traditional basic CS (chapter 4), CS with prior information (section 5.1) [42], and modified CS with prior information (section 5.2). In traditional basic CS, CS with prior information and modified CS with prior information, partial sampling is employed at the receiver end. A key novelty of this work is the two-dimensional Fourier domain representation of the underwater acoustic channel, that enables localization of slowly-varying channel components against transient and potentially high-energy taps due to ephemeral oceanic events. For the current 2D Fourier domain setting, traditional basic CS within this framework (Figures 4.2 and 4.3) and least squares with sparsity regularization (Direct denoising framework) are considered as the base performance standards to ensure fair comparison against the state-of-the-art.

Fig. 5.10 and 5.11 present NMSE results of estimated channel with different window lengths and varying sampling ratios for noisy channel SNR of 10dB and 5dB, respectively. It is observed that the *modified CS with prior information*, i.e., with full sampling of zero Doppler, (5.3) provides best performance with marginal performance gap between 40% and 100% sampling ratios. This is to be expected given the results and related discussions in Sections 5.1 and 5.2

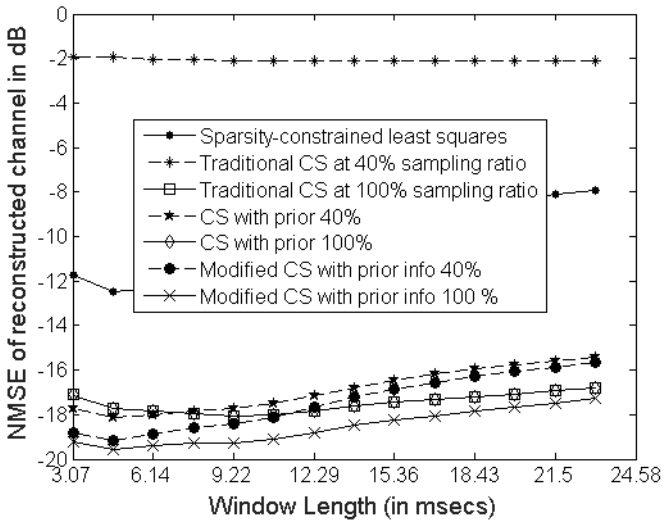

Figure 5.10: Comparative performance of channel estimation with different sparse sensing techniques at 10dB SNR; Results on modified CS with prior relate to full sampling of zero Doppler.

5.4 Results on Simulated channel

In order to demonstrate the efficacy of the proposed method, this section presents results on a public-domain simulated channel that emulates multipath channel effects. This channel

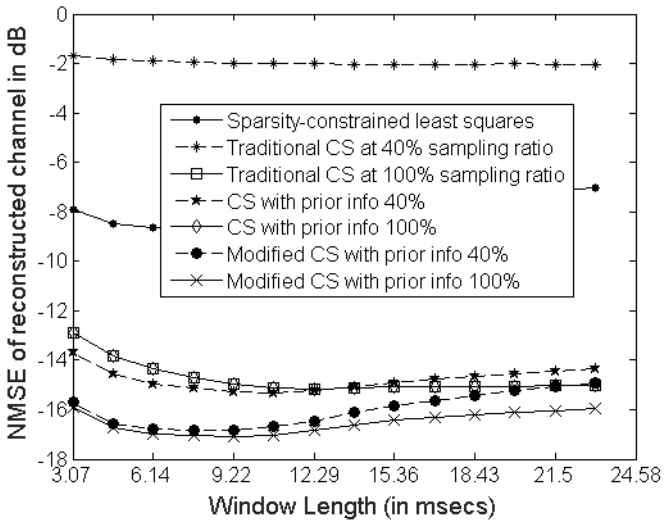

Figure 5.11: Comparative performance of channel estimation at 5dB SNR; Results on modified CS with prior relate to full sampling of zero Doppler.

simulator has been proposed recently [3,4] and is unrelated to channel estimates used in previous sections. This channel simulator models different multipath effects commonly encountered in shallow water acoustic communications, and has also successfully interpreted specular reflections and multipath arrivals in shallow water channel across several field trials [3,4] including SPACE08 and other experimental channel data. Channel parameters used in this simulation work are presented in Appendix. A two-dimensional delay-time snapshot of channel for 0.5sec duration is shown in Fig. 5.12 with corresponding 2D Fourier domain representation shown in Fig. 5.13.

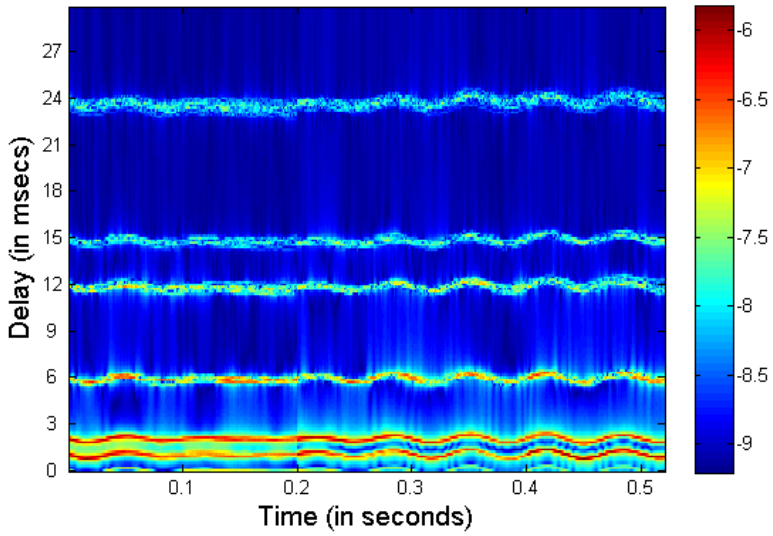

Figure 5.12: Simulated Channel in delay-time (2D time domain) using Channel Simulator [4]; colorbar is in log scale.

Figures 5.12 and 5.13 clearly show that this channel is very distinct from the NCMNS

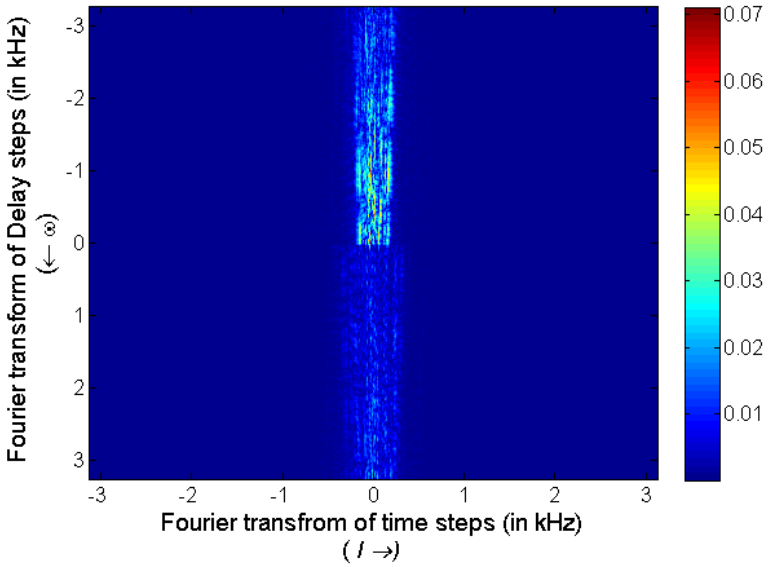

Figure 5.13: Simulated Channel of Fig. 5.12 in 2D Fourier domain; colorbar is in linear scale.

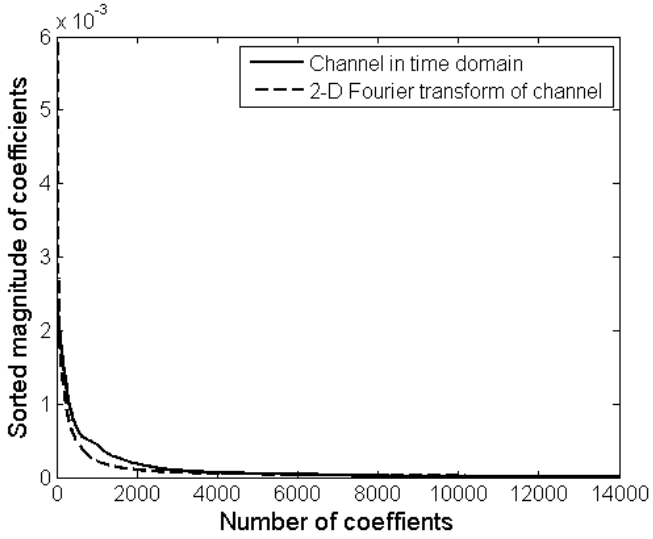

Figure 5.14: Sorted magnitude coefficients of 2-D time domain channel shown in Fig. 5.12 and 2-D Fourier transform of channel shown in Fig. 5.13.

channel estimates used for numerical simulations setup in previous sections (refer to Figures 1.1 and 1.2). Figure 5.14 shows sorted magnitude of 2D time domain and 2D frequency domain channel coefficients. Compared to the 2D time-domain, this channel is also more sparse in the 2D frequency domain, although the relative sparsity is less compared to the previous SPACE08 experimental data.

Channel estimation results are presented on this channel with modified CS with prior information. As evident from Fig. 5.13, this channel is dense at zero Doppler and few low Doppler frequencies. Hence, the support T is considered to be zero Doppler and first five Doppler frequencies. NMSE estimation results are presented for noisy channel SNR of 10dB and 5dB in

Figures 5.15 and 5.16, and correspond to results presented in Figures 5.8 and 5.9, which were based on simulations using NCMNS estimates on SPACE08 field data (200 meters range, 15 meters depth, moderate sea conditions). Similar to the results on previous channel (Figures 5.8 and 5.9), good results are obtained with the proposed non-uniform modified CS with prior information.

It is observed that for this independent numerical experiment, the NMSE variation shows two consistent similarities between Figures 5.8 and 5.15: (i) NMSE performance of all sampling ratios converge up to a critical averaging window, which represents the minimum observation length to capture the dominant "steady-state", i.e., slowly varying channel components corresponding to low Doppler frequencies. (ii) While the lowest NMSE is obtained for the highest sampling rate, the difference in NMSE performance between different sampling ratios is within 1dB for observation windows close to this critical window length.

Lowering SNR increases the ambient noise levels, and therefore, the convergence effect around the critical window length is reduced in Figures 5.9 and 5.16. However, the convergence effect is still seen in Figure 5.16, for the channel in Figure 5.12, which has significantly less lower-magnitude channel components from diffused reflection, and therefore, less vulnerable to low SNR issues.

The principal difference between the NMSE results for the two types of channels (Figures 1.1 and 5.12) is that for the simulated channel (Figure 5.12), NMSE decreases for increasing window length (refer Figures 5.15 and 5.16). This is because this channel has more slowly varying channel components due to relatively steady multipath arrivals from specular reflections. Therefore, for the simulated channel (Figure 5.12) the slowly varying components occupying the lower Doppler frequencies, as seen in Figure 5.13, dominate the two-dimensional Fourier domain than the estimated channel in Figure 1.1. Therefore, Figures 5.15 and 5.16 exhibit improvement in NMSE as the averaging window length increases whereas Figures 5.8 and 5.9 show an optimal window length where NMSE is minimized before increasing again. It is noteworthy that for sufficiently long window lengths similar minima is expected for Figures 5.15 and 5.16 as well, as the gain in high-precision estimation of the steady-state components is slowly offset by the loss in precision to capture the transient variations.

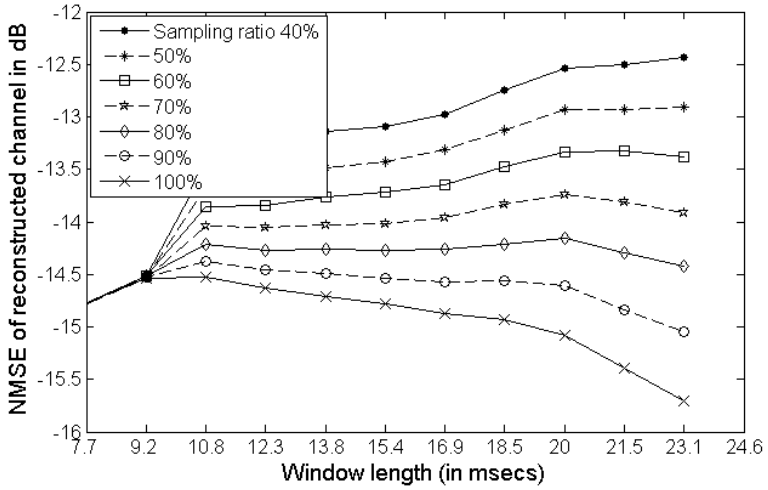

Figure 5.15: NMSE results on channel estimation at 10dB SNR with **modified CS**, support T is **zero and first five non-zero Doppler frequencies**; implements (5.3).

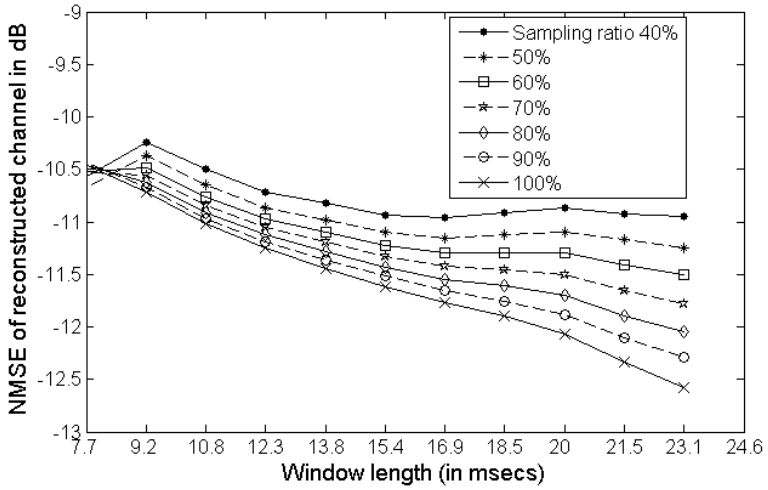

Figure 5.16: NMSE results on channel estimation at 5dB SNR with **modified CS**, support T is **zero and first five non-zero Doppler frequencies**; implements (5.3).

Chapter 6

Underwater Channel Estimation with Energy Efficient Dictionary Transmission

This chapter presents energy efficient partial transmission that builds on the channel estimation framework. From an energy-efficiency perspective, higher frequency transients typically occupy less energy than the direct arrival $U[0,\omega]_{\omega=0}^{K-1}$ and therefore, the input signal dictionary can be designed to detect more activity around the direct arrival and primary multipath region, with partial sampling along the secondary multipath region. The trade-off between energy-efficiency and performance will be given by the relative performance margins of the sampling ratios chosen.

6.1 Energy Efficient Dictionary Transmission- Partial Transmission of Dictionary Atoms

Consider (3.3) where K possible delay frequencies $\omega = 0, 1, \ldots, K-1$ based input dictionary atoms of complex exponential $x[i,\omega] = e^{j\frac{2\pi i\omega}{K}}$ are transmitted across K parallel sub-channels. Let us say only $S\%$ of dictionary atoms are required to be transmitted, i.e., K' sub-channels being selected randomly, where $K' = \lfloor \frac{K\times S}{100} \rfloor$. On carrying out post-processing similar to equations (3.2) and (3.3), we can write (3.4) in the case of energy efficient transmission as:

$$\mathbf{U}_{sub} = \tilde{\mathfrak{R}}\mathfrak{F}\mathbf{H}, \tag{6.1}$$

where $\tilde{\mathfrak{R}}$ is the operator that translates fewer dictionary atom transmissions into restriction operator on $\mathfrak{F}\mathbf{H}$. Since the channel is noisy, received signal is represented by

$$\mathbf{U}_{sub} = \tilde{\mathfrak{R}}\mathfrak{F}\mathbf{H} + \mathbf{N}, \tag{6.2}$$

where $\mathbf{N}$ is the complex white Gaussian noise matrix. The channel can be estimated by solving the following LASSO optimization problem:

$$\underset{\mathbf{U}}{min}||\mathbf{U}_{sub} - \tilde{\mathfrak{R}}\{\mathbf{U}\}||_2^2 \quad \text{subject to } ||\mathbf{U}||_1 \leq \tau, \tag{6.3}$$

where $\mathbf{U} = \mathfrak{F}\mathbf{H}$. From Fig. 1.2 it can be noted that the zero Doppler frequency in the 2D Fourier domain of the channel corresponds to the most dominant steady component of the channel. Hence, zero Doppler frequency or center column of $\mathbf{U}$ contains most of the energy, while other Doppler frequencies contain relatively less energy and are more sparse than zero Doppler frequency. Hence, it is proposed to fully sense the zero Doppler (center column of $\mathbf{U}$) called the support T and partially sense the remaining Doppler frequencies (or the rest of the columns of $\mathbf{U}$) denoted as the support T^c. Now, by imposing sparsity on T^c, the channel estimation problem is set-up in the framework of modified CS with no partial sampling in the dominant zero Doppler frequency component of the channel. Hence, $\mathbf{U}_{sub}$ in (6.1) is modified as $\mathbf{U}_{sub,ext}$ to incorporate the information of the center column of $\mathbf{U}$ and (6.3) is re-written in the modified CS framework as below:

$$\underset{\mathbf{U}}{min}||\mathbf{U}_{sub,ext} - \tilde{\mathfrak{R}}_{ext}\{\mathbf{U}\}||_2^2 \quad \text{subject to } ||\mathbf{U}_{T^c}||_1 \leq \tau, \tag{6.4}$$

where $\tilde{\mathfrak{R}}_{ext}$ is the extension of operator $\tilde{\mathfrak{R}}$ that allows inclusion of information corresponding to the center column of $\mathbf{U}$ in $\mathbf{U}_{sub,ext}$.

6.2 Results

Figures 6.1 and 6.2 show simulation results over 200 iterations at different sampling ratios (S) ranging from 40% to 100% on the channel described above for noise levels at 10dB and 5dB, respectively. From these figures, it is observed that the performance gap between 100% and 40% sampling ratio is approx. 0.5 to 1 dB until the optimal observation window where minimal NMSE is obtained for all sampling ratios. This optimal observation window represents the minimal time of observation necessary to estimate the dominant low frequency components and as such, should be independent of the sampling ratio. Fig. 6.1 and 6.2, respectively, record this optimal observation window length at 30 time samples ($\sim$4.6 milliseconds) for 10 dB SNR and 60 time samples ($\sim$9 milliseconds) for 5 dB SNR. These minima also represent optimal trade-off between energy efficiency and channel estimator performance. Further, 100% sampling ratio that represents the non-compressed dictionary, dominates NMSE performance as seen in Fig. 6.1 and 6.2. This is primarily due to superior ability of higher sampling ratios to correctly estimate transients that are locally dominant but not as high-energy as the steady-state low-Doppler components. Thus, we conclude that robust channel estimation under energy efficient transmitted dictionaries is best achieved when the transmitted codebook correctly captures the underlying support of the channel.

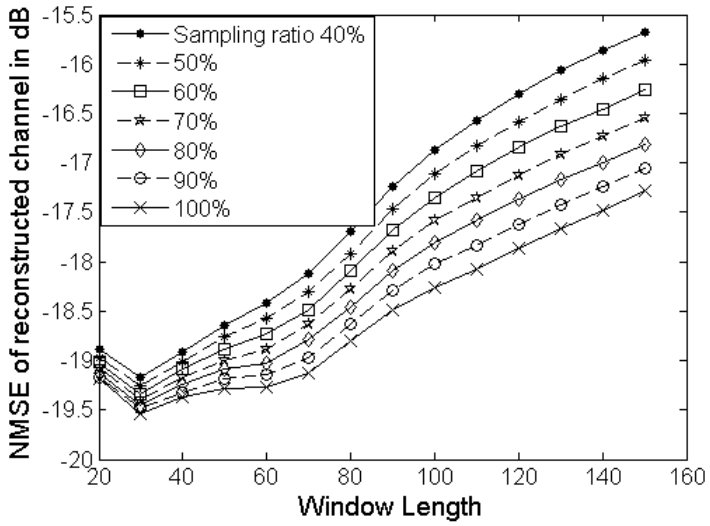

Figure 6.1: NMSE for channel estimates using (6.3) with noisy channel SNR=10dB with modified CS recovery framework and transmission of dictionary elements over fewer frequency sub-channels; Support T corresponds to zero Doppler component; Window length is in number of time samples.

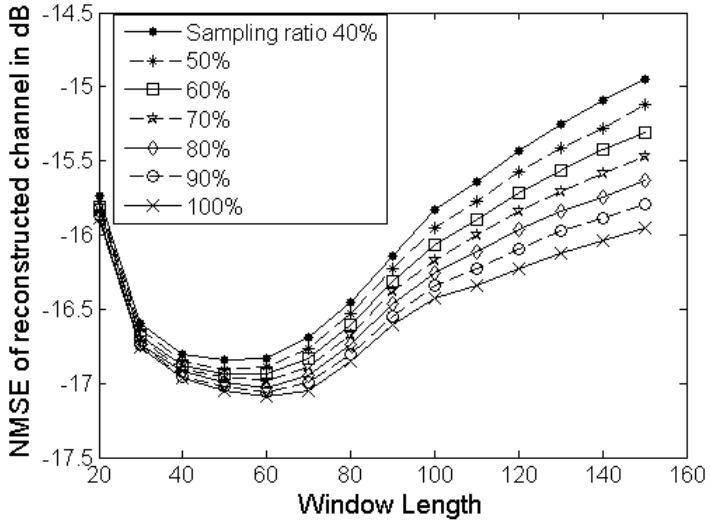

Figure 6.2: NMSE for channel estimates using (6.3) with noisy channel SNR=5dB with modified CS and transmission of dictionary elements over fewer frequency sub-channels; Support T corresponds to zero Doppler component; Window length is in number of time samples.

Chapter 7

Conclusion and Future Work

7.1 Conclusion

A two-dimensional frequency domain representation is introduced that captures the time-varying fluctuations of the shallow water acoustic channel both in delay frequency and Doppler frequencies. The chief advantage of choosing this two-dimensional frequency domain is that it disambiguates the slowly varying channel components which occupy the lower frequency bands, against the transient channel components, which are difficult to model or predict, and typically occupy the higher frequency bands. Furthermore, the transient channel components occupying the higher frequencies typically manifest a sparser distribution locally, than their slowly varying counterparts in the lower frequency bands. This disambiguation of diverse channel effects within the two-dimensional spectra is exploited to introduce non-uniform compressive sampling, where different sampling ratios are employed at different frequency bands to take advantage of the relative sparsity of different types of channel components. This work is scoped to the channel estimation aspects with no feedback or iteration between transmitter and receiver. Proposed methods are validated through extensive numerical simulations. These numerical experiments employ two independent channels as the simulation setup: (i) field estimates from the SPACE08 experiment using established techniques, as well as (ii) a public-domain channel simulator that emulates well-known oceanic phenomena such as specular reflections, and have been tested against real channel estimates from field trials. Overall, the conclusion of these investigations show consistent results between the two types of independent numerical experimentation. Simulation results demonstrate that the optimal operating point of channel observation is an intricate combination of observation window length, local sparsity of the channel support (e.g. within a given frequency band), as well as the sampling ratio appropriate for that local (and typically unknown in advance) sparsity. An adaptive technique is also provided that heuristically estimates the locally optimal operating point by minimizing the normalized prediction error for the estimated channel locally. Simulation results also demonstrate that while, as expected the normalized mean squared error improves with increasing sampling ratio, the performance gap between high and low sampling ratios is within 1 dB when operating around (or close to) this

optimal operating point. This is well-known in compressive sampling, where the primary gain is achieveing similar error rates using drastically smaller sampling ratios. This work articulates the same concept for shallow water acoustic communications, and introduces a non-uniform compressive sampling framework in a two-dimensional frequency domain, that is cognizant of the fundamentally intertwined nature of the shallow water acoustic channel: between non-stationary transient elements, and relatively steady channel components due to diverse multipath phenomena.

7.2 Limitations and Future Work

7.2.1 Limitations

Following are the limitations of the work done:

a. We have used only two channels as ground truth, one is NCMNS (non convex mixed norm solver) based channel estimates of SPACE08 experimental field data and other one is simulated channel obtained from publicly available channel simulator4,5. The numerical experiments could have been performed on more number of channels.

b. The observations are made based on the two channel described above. The observations could have generalized based on more number of channels.

c. The results of non-uniform compressed sensing proposed in the paper are compared only with the basic compressed sensing techniques and sparsity constrained least squares. Results are not compared with other existing methods in literature.

7.2.2 Future Work

Some of the potential future directions of the work are described below:

a. The proposed method is tested on two channels, one SPACE08 channel estimate and another one is simulated channel. Experiments can be performed on more number of channels instead of just two above, in different sea conditions like high and low wind activity, calm and highly rough sea conditions and hence, the observations made in the work can be generalized. Also, the results of the proposed methods can be compared with the existing state of the art.

b. The experiments can be performed in real scenario where channel in not known apriori.

c. The concept of non-uniform compressed sensing can also be explored in delay-Doppler domain (where delay is in time domain and Doppler is in frequency domain).

Publications

- Naushad Ansari, Anubha Gupta, and Ananya Sen Gupta, "Shallow water acoustic channel estimation using two-dimensional frequency characterization", In *Journal of Acoustic Society of America (JASA), Accepted*, 2016.
- Naushad Ansari, Anubha Gupta, and Ananya Sen Gupta, "Physics inspired CS based underwater acoustic channel estimation". In *Global Conference on Signal and Information Processing (GlobalSIP)*, pages 1106-1110. IEEE, Dec 2015.
- Ananya Sen Gupta, Naushad Ansari, and Anubha Gupta. "Tracking the underwater acoustic channel using two-dimensional frequency sampling". In *International Symposium on Underwater Technology (ISUT)*, pages 1–5. IEEE, 2015.
- Naushad Ansari, Ananya Sen Gupta and Anubha Gupta. "Underwater Channel Estimation with Energy Efficient Dictionary Transmission". In *IEEE Signal Processing Letters, Communicated*. IEEE, 2017.

Appendix A

Below is the list of parameters used to simulate an underwater acoustic channel used in Section 5.4 (refer to Figure 5.12 generated using [3], with the help of MATLAB code present at [4]

h0=103; (surface height (depth) [m])
ht0=58; (Transmitter height [m])
hr0=59; (Receiver height [m])
d0=3000; (channel distance [m])

k=1.7; (spreading factor)
c=1500; (speed of sound in water [m/s])
c2=1200; (speed of sound in bottom [m/s] (>1500 for hard, < 1500 for soft))
cut=20; (do not consider arrivals whose strength is below that of direct arrival divided by cut)

fmin=8.5e3; (minimum frequency [Hz])
B=9e3; (bandwidth [Hz])

df= 25; (frequency resolution [Hz], f_vec=fmin:df:fmax;)

dt= 50e-3; (time resolution [seconds])
T_SS=60; (coherence time of the small-scale variations [seconds])

Small-Scale (S-S) parameters:
sig2s= 1.125; (variance of S-S surface variations)
sig2b=sig2s/2; (variance of S-S bottom variations)

B_delp= 5e-4; (3-dB width of the p.s.d. of intra-path delays (assumed constant for all paths))
Sp= 20; (number of intra-paths (assumed constant for all paths)
mu_p= .5/Sp; (mean of intra-path amplitudes (assumed constant for all paths))
nu_p= 1e-6; (variance of intra-path amplitudes (assumed constant for all paths))

Large-Scale (L-S) parameters:
T_tot= 3*T_SS; (total duration of the simulated signal [seconds])
t_tot_vec=(0:dt:T_tot); Lt_tot=length(t_tot_vec);

h_bnd=[-10 10]; (range of surface height variation (L-S realizations are limited to h+h_band))
ht_bnd=[-5 5]; (range of transmitter height variation)
hr_bnd=[-5 5]; (range of receiver height variation)
d_bnd=[-20 20]; (range of channel distance variation)

sig_h=1; (standard deviation of L-S variations of surface height)
sig_ht=1; (standard deviation of L-S variations of transmitter height)
sig_hr=1; (standard deviation of L-S variations of receiver height)
sig_d=1; (standard deviation of L-S variations of distance height)
a_AR= .9; (AR parameter for generating L-S variations (constant for variables h, ht, hr, d))

Bibliography

[1] B. Tomasi, J. Preisig, G. B. Deane, and M. Zorzi, "A study on the wide-sense stationarity of the underwater acoustic channel for non-coherent communication systems," in *Wireless Conference 2011-Sustainable Wireless Technologies (European Wireless), 11th European*. VDE, 2011, pp. 1–6.

[2] A. S. Gupta and J. Preisig, "A geometric mixed norm approach to shallow water acoustic channel estimation and tracking," *Physical Communication*, vol. 5, no. 2, pp. 119–128, 2012.

[3] P. Qarabaqi and M. Stojanovic, "Statistical characterization and computationally efficient modeling of a class of underwater acoustic communication channels," *Oceanic Engineering, IEEE Journal of*, vol. 38, no. 4, pp. 701–717, 2013.

[4] ——, "Acoustic channel modeling and simulation," http://millitsa.coe.neu.edu/?qprojects.

[5] D. L. Donoho, "For most large underdetermined systems of linear equations the minimal $l1$-norm solution is also the sparsest solution," *Communications on pure and applied mathematics*, vol. 59, no. 6, pp. 797–829, 2006.

[6] C. R. Berger, S. Zhou, J. C. Preisig, and P. Willett, "Sparse channel estimation for multicarrier underwater acoustic communication: From subspace methods to compressed sensing," *Signal Processing, IEEE transactions on*, vol. 58, no. 3, pp. 1708–1721, 2010.

[7] W. Li and J. C. Preisig, "Estimation of rapidly time-varying sparse channels," *Oceanic Engineering, IEEE Journal of*, vol. 32, no. 4, pp. 927–939, 2007.

[8] M. H. Hayes, *Statistical Digital Sig. Proc. and Modeling*. Wiley, 1996.

[9] S. S. Haykin, *Adaptive filter theory*. Pearson Education India, 2008.

[10] A. S. Gupta, "Time-frequency localization issues in the context of sparse process modeling," in *Proceedings of Meetings on Acoustics*, vol. 19, no. 1. Acoustical Society of America, 2013, p. 070084.

[11] M. Stojanovic, J. Proakis, and J. Catipovic, "Analysis of the impact of channel estimation errors on the performance of a decision-feedback equalizer in fading multipath channels," *IEEE Trans. Commun. COM*, vol. 43, pp. 877–886, 1995.

[12] E. V. Zorita and M. Stojanovic, "Space-frequency block coding for underwater acoustic communications," *Oceanic Engineering, IEEE Journal of*, vol. 40, no. 2, pp. 303–314, 2015.

[13] A. Radosevic, R. Ahmed, T. M. Duman, J. G. Proakis, and M. Stojanovic, "Adaptive OFDM modulation for underwater acoustic communications: Design considerations and experimental results," *Oceanic Engineering, IEEE Journal of*, vol. 39, no. 2, pp. 357–370, 2014.

[14] Y. M. Aval and M. Stojanovic, "Differentially coherent multichannel detection of acoustic OFDM signals," *Oceanic Engineering, IEEE Journal of*, vol. 40, no. 2, pp. 251–268, 2015.

[15] B. Li, S. Zhou, M. Stojanovic, L. Freitag, and P. Willett, "Multicarrier communication over underwater acoustic channels with nonuniform Doppler shifts," *Oceanic Engineering, IEEE Journal of*, vol. 33, no. 2, pp. 198–209, 2008.

[16] E. Calvo and M. Stojanovic, "Efficient channel-estimation-based multiuser detection for underwater CDMA systems," *Oceanic Engineering, IEEE Journal of*, vol. 33, no. 4, pp. 502–512, 2008.

[17] M. Chitre, "A high-frequency warm shallow water acoustic communications channel model and measurements," *The Journal of the Acoustical Society of America*, vol. 122, no. 5, pp. 2580–2586, 2007.

[18] P. Bello *et al.*, "Characterization of randomly time-variant linear channels," *Communications Systems, IEEE transactions on*, vol. 11, no. 4, pp. 360–393, 1963.

[19] J. C. Preisig and G. B. Deane, "Surface wave focusing and acoustic communications in the surf zone," *The Journal of the Acoustical Society of America*, vol. 116, no. 4, pp. 2067–2080, 2004.

[20] A. S. Gupta and J. Preisig, "Tracking the time-varying sparsity of channel coefficients in shallow water acoustic communications," in *Signals, Systems and Computers (ASILOMAR), 2010 Conference Record of the Forty Fourth Asilomar Conference on.* IEEE, 2010, pp. 1047–1049.

[21] ——, "Adaptive sparse optimization for coherent and quasi-stationary problems using context-based constraints," in *Acoustics, Speech and Signal Processing (ICASSP), 2012 IEEE International Conference on.* IEEE, 2012, pp. 3413–3416.

[22] S. F. Cotter and B. D. Rao, "Sparse channel estimation via matching pursuit with application to equalization," *Communications, IEEE Transactions on*, vol. 50, no. 3, pp. 374–377, 2002.

[23] J. Huang, J. Huang, C. R. Berger, S. Zhou, and P. Willett, "Iterative sparse channel estimation and decoding for underwater MIMO-OFDM," *EURASIP Journal on Advances in Signal Processing*, vol. 2010, p. 1, 2010.

[24] K. Pelekanakis and M. Chitre, "New sparse adaptive algorithms based on the natural gradient and the-norm," *Oceanic Engineering, IEEE Journal of*, vol. 38, no. 2, pp. 323–332, 2013.

[25] P. C. Carrascosa and M. Stojanovic, "Adaptive channel estimation and data detection for underwater acoustic MIMO-OFDM systems," *Oceanic Engineering, IEEE Journal of*, vol. 35, no. 3, pp. 635–646, 2010.

[26] E. J. Candes, J. K. Romberg, and T. Tao, "Stable signal recovery from incomplete and inaccurate measurements," *Communications on pure and applied mathematics*, vol. 59, no. 8, pp. 1207–1223, 2006.

[27] J. Tropp, A. C. Gilbert *et al.*, "Signal recovery from random measurements via orthogonal matching pursuit," *Information Theory, IEEE Transactions on*, vol. 53, no. 12, pp. 4655–4666, 2007.

[28] D. Needell and J. A. Tropp, "CoSaMP: Iterative signal recovery from incomplete and inaccurate samples," *Applied and Computational Harmonic Analysis*, vol. 26, no. 3, pp. 301–321, 2009.

[29] R. Tibshirani, "Regression shrinkage and selection via the lasso," *Journal of the Royal Statistical Society. Series B (Methodological)*, pp. 267–288, 1996.

[30] D. L. Donoho, "Compressed sensing," *Information Theory, IEEE Transactions on*, vol. 52, no. 4, pp. 1289–1306, 2006.

[31] E. J. Candès, "The restricted isometry property and its implications for compressed sensing," *Comptes Rendus Mathematique*, vol. 346, no. 9, pp. 589–592, 2008.

[32] E. J. Candes and Y. Plan, "A probabilistic and RIPless theory of compressed sensing," *Information Theory, IEEE Transactions on*, vol. 57, no. 11, pp. 7235–7254, 2011.

[33] N. Vaswani and W. Lu, "Modified-CS: Modifying compressive sensing for problems with partially known support," *Signal Processing, IEEE Transactions on*, vol. 58, no. 9, pp. 4595–4607, 2010.

[34] M. Lustig, D. L. Donoho, J. M. Santos, and J. M. Pauly, "Compressed sensing mri," *IEEE Signal Processing Magazine*, vol. 25, no. 2, pp. 72–82, 2008.

[35] M. Lustig, D. Donoho, and J. M. Pauly, "Sparse mri: The application of compressed sensing for rapid mr imaging," *Magnetic resonance in medicine*, vol. 58, no. 6, pp. 1182–1195, 2007.

[36] E. Van den Berg and M. P. Friedlander, "Sparse optimization with least-squares constraints," *SIAM Journal on Optimization*, vol. 21, no. 4, pp. 1201–1229, 2011.

[37] E. van den Berg and M. P. Friedlander, "Probing the Pareto frontier for basis pursuit solutions," *SIAM Journal on Scientific Computing*, vol. 31, no. 2, pp. 890–912, 2008. [Online]. Available: http://link.aip.org/link/?SCE/31/890

[38] ——, "SPGL1: A solver for large-scale sparse reconstruction," June 2007, http://www.cs.ubc.ca/labs/scl/spgl1.

[39] J. Romberg, "Imaging via compressive sampling [introduction to compressive sampling and recovery via convex programming]," *IEEE Signal Processing Magazine*, vol. 25, no. 2, pp. 14–20, 2008.

[40] E. J. Candès, J. Romberg, and T. Tao, "Robust uncertainty principles: Exact signal reconstruction from highly incomplete frequency information," *Information Theory, IEEE Transactions on*, vol. 52, no. 2, pp. 489–509, 2006.

[41] A. S. Gupta, N. Ansari, and A. Gupta, "Tracking the underwater acoustic channel using two-dimensional frequency sampling," in *Underwater Technology (UT)*. IEEE, 2015, pp. 1–5.

[42] N. Ansari, A. Gupta, and A. S. Gupta, "Physics inspired CS based underwater acoustic channel estimation," in *GlobalSIP 2015 (Accepted)*. IEEE.